Lithos 226 (2015) 233–254

Contents lists available at ScienceDirect

Lithos

journal homepage: www.elsevier.com/locate/lithos

Accretion, underplating and exhumation along a subduction interface: From subduction initiation to continental subduction (Tavşanlı zone, W. Turkey)

Alexis Plunder [a,b,c,*], Philippe Agard [b,c,d], Christian Chopin [a], Amaury Pourteau [e], Aral I. Okay [f]

[a] Laboratoire de Géologie, Ecole Normale Supérieure, UMR CNRS 8538, 24 rue Lhomond, 75005, Paris, France
[b] Sorbonne Universités, UPMC Univ Paris 06, UMR 7193, ISTeP, F-75005, Paris, France
[c] CNRS, UMR 7193, ISTeP, F-75005, Paris, France
[d] IUF, F-75005, Paris, France
[e] Institut für Erd- und Umweltwissenschaften, Universität Potsdam, Karl–Liebknecht–Straße 24–25, Potsdam–Golm, 14476, Germany
[f] Eurasia Institute of Earth Sciences and Department of Geology, Istanbul Technical University, Maslak, 34469 Istanbul, Turkey

ARTICLE INFO

Article history:
Received 14 June 2014
Accepted 10 January 2015
Available online 22 January 2015

Keywords:
Subduction interface
PT estimates
HP-LT rocks
Accretion, underplating and exhumation processes

ABSTRACT

We herein reappraise the pressure–temperature (PT) evolution of the high-pressure and low-temperature (HP–LT) Tavşanlı zone (western Turkey) in order to (i) better characterize rock units exhumed along a cooling subduction interface, from birth to steady state and (ii) constrain exhumation and detachment dynamics, as well as mechanical coupling between plates. Based on PT estimates and field observations three oceanic complexes are recognized between the HP–LT continental margin and the obducted ophiolite, with PT estimates ranging from incipient metamorphism to blueschist-facies conditions. PT conditions for the continental unit are reappraised to 24 kbar and ~500 °C on the basis of pseudosection modelling and Raman spectroscopy on carbonaceous material. A tentative reconstruction of the subduction zone evolution is proposed using available radiometric and palaeogeographic data and recent thermomechanical modelling. Both PT conditions and field observations point out to the slicing of km-sized units at different preferred depths along the subduction interface, thus providing constraints on the dynamics of accretion and underplating. In particular, the comparison of PT estimates for the Tavşanlı zone and for other broadly similar fossil subduction settings (i.e., Oman, Corsica, New Caledonia, Franciscan, Schistes Lustrés) suggests that units are detached preferentially from the slab at specific depths of 30-40 km (i.e., downdip of the seismogenic zone) and ~80 km. We propose that these depths are controlled by major changes in mechanical coupling along the plate interface, whereas exhumation through time would rather be controlled by large-scale geodynamic boundary conditions.

1. Introduction

The thermal state of present-day subduction zones is well constrained by studies coupling heat flow (Hyndman and Peacock, 2003; Wada and Wang, 2009), seismicity (Hacker et al., 2003; Kirby et al., 1996; Peacock and Wang, 1999) and numerical modelling (Abers et al., 2006; Syracuse et al., 2010; van Keken et al., 2011). Several numerical models have also investigated the progressive cooling of subduction zone after subduction initiation (Gurnis et al., 2004; Hacker, 1990, 1991). The natural record of evolving geotherms within long-lived subduction zones, however, is presently lacking.

High-pressure–low-temperature (HP–LT) rocks convey information that can help to retrieve the different steps of subduction evolution: they do not only preserve the record of thermal conditions at depth but also information on mechanical coupling, transfer of mass and fluids along the subduction interface, or on the mechanism of subduction initiation (Agard and Vitale-Brovarone, 2013; Agard et al., 2009; Angiboust et al., 2012; Hacker, 1990; Marschall and Schumacher, 2012; Wada and Wang, 2009).

The Tavşanlı zone (western Turkey), with fragments of both HP–LT oceanic and thinned continental material subducted beneath a large-scale ophiolite (i.e., a piece of obducted oceanic lithosphere), potentially provides an exceptional record of such successive subduction steps (Okay et al., 1998; Plunder et al., 2013): (1) initiation of the intra-oceanic subduction, as witnessed by a high-temperature metamorphic sole at the base of the ophiolite (Okay et al, 1998; Önen and Hall, 1993); (2) subsequent oceanic subduction, fossilized by the presence of an oceanic accretionary complex with varied HP–LT rocks (Okay, 1982; Plunder et al., 2013); (3) the subduction of the continental margin as attested by uncommon high-pressure jadeite-glaucophane-chloritoid-lawsonite-bearing sedimentary and felsic rocks (Okay and

* Corresponding author at: Sorbonne Universités, UPMC Univ Paris 06, UMR 7193, ISTeP, F-75005, Paris, France.
E-mail address: alexis.plunder@upmc.fr (A. Plunder).

http://dx.doi.org/10.1016/j.lithos.2015.01.007
0024-4937/

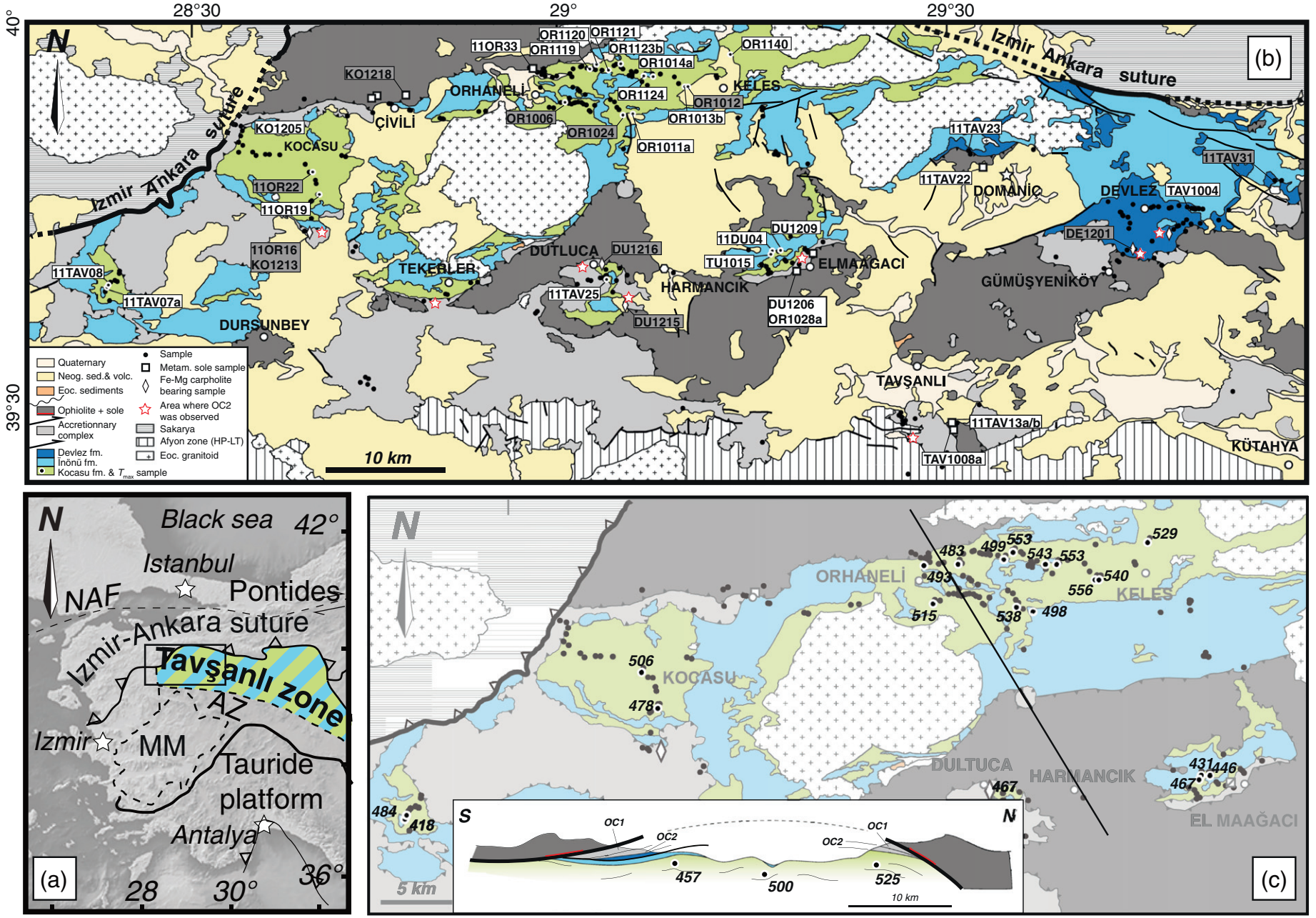

Fig. 1. (a) Tectonic map of western Anatolia showing the position of the Tavşanlı zone and of the studied area. AZ, Afyon zone; MM, Menderes massif. Modified from Jolivet et al. (2013); Moix et al. (2008); Okay and Tüysüz (1999); Pourteau et al. (2013). Topography from Geomapapp 3.3.6 (http://www. geomapapp.org/). (b) Simplified geological map of the western part of the Tavşanlı zone with location of the samples mentioned in text or in other figures. Modified from MTA (2002). (c) Simplified structural sketch of the westernmost part of the field area with maximum temperature determined by Raman spectroscopy on carbonaceous material. Inset represents a simplified cross-section.

Kelley, 1994; Okay et al., 2008). Importantly, these rocks are also devoid of later collisional imprint.

Using pseudosection modelling (and testing most recent thermodynamic models for HP-LT rocks) we herein provide new PT estimates for the Tavşanlı zone with the following specific aims: (a) gather a comprehensive set of estimates for rock remnants of all subduction steps (i.e., intra-oceanic subduction, oceanic and then continental subduction), (b) provide clues on the progressive regional-scale structuration of the Tavşanlı zone and (c) document accretionary and exhumation processes during the cooling of a subduction zone, from its birth to continental subduction.

2. Geological setting

The geological setting of Western Anatolia and Tavşanlı zone is reviewed in numerous publications (e.g. Candan et al., 2005; Moix et al., 2008; Okay and Tüysüz, 1999; Pourteau et al., 2010, 2013; Şengör and Yılmaz, 1981; van Hinsbergen et al., 2010); only essential information is recalled here. The reader is referred to Plunder et al. (2013) for further details on the local geology, age constraints, and detailed tectonic evolution.

2.1. Western Anatolia

The İzmir–Ankara suture zone (Fig. 1a) marks the closure of the Neotethyan ocean which once separated Laurasia- to the north from Gondwana-related terranes to the south during mid-late Triassic to late Cretaceous–Palaeogene times (Barrier and Vrielynck, 2008; Dercourt et al., 1993; Robertson et al., 1996). North of the suture are the Pontides, characterised by pre-Jurassic metamorphic rocks, unconformably overlain by non-metamorphosed Jurassic to Cretaceous volcanic and sedimentary rocks (Altiner et al., 1991; Okay et al., 2013). South of the İzmir-Ankara suture the Anatolide-Tauride Block is made of metamorphic and non-metamorphic Precambrian to Eocene rocks (Okay and Tüysüz, 1999; Şengör and Yılmaz, 1981). In these Gondwana-derived continental domains, three major metamorphic zones are commonly distinguished from north to south: the Tavşanlı zone, the Afyon zone and the Menderes massif (Fig. 1a). For more information about palaeogeography and geodynamics of Western Anatolia, readers are referred to Moix et al. (2008), Okay and Tüysüz (1999), Pourteau et al. (2013), Şengör and Yılmaz (1981), van Hinsbergen et al. (2010) and references cited therein.

2.2. The Tavşanlı zone

The Tavşanlı zone is an east-west trending, 250–300 km long and ~50 km wide belt, (Fig. 1a). It is made of a Palaeozoic to Mesozoic sedimentary sequence similar to the one observed in Afyon and Menderes units (Permo-Triassic clastics and thick platform-type Mesozoic marble; Candan et al., 2005; Moix et al., 2008; Okay and Tüysüz, 1999; Okay et al., 2008) for which a Gondwana-derived origin is inferred (Candan et al., 2005; Gessner et al., 2004). The Tavşanlı zone thus corresponds to the northern passive continental margin of the Anatolide-Tauride Block subducted below an oceanic plate during the late Cretaceous (Okay, 1986; Okay et al., 1998; Önen and Hall, 1993). Three main tectonic units can be recognized in the Tavşanlı zone *sensu lato*, from top to bottom: (1) an ophiolitic unit obducted over the continental margin; (2) a Cretaceous accretionary complex (made of Neotethyan oceanic material); and (3) the Orhaneli sequence, which corresponds to the Tavşanlı zone *sensu stricto* (Fig. 1b). Their approximate respective volumes are indicated in the cross-section of Fig. 1. The stacking of units in the Tavşanlı Zone and details on structural thicknesses for ocean-derived units are specified in Section 7.2.

(1) The main ophiolitic body rests atop the Orhaneli sequence and the accretionary complex (Fig. 1; Lisenbee, 1972; Okay, 1980a, 1980b, 1982; Plunder et al., 2013). The peridotite thrust sheet crops out as numerous klippen of partly serpentinized harzburgite and dunite (up to 90%), with minor (<10%) pyroxenite, chromitite, diabase, and gabbro (Lisenbee, 1972; Önen, 2003). A supra-subduction zone signature was documented for the ophiolite, supporting the formation in a fore-arc context (Manav et al., 2004; Önen, 2003; Sarıfakıoğlu et al., 2009) although the geochemistry data refer only to isolated late diabase dikes post-dating the formation of the sole (Önen, 2003). Slices of amphibolite-facies metamorphic rocks can be found in places at the base of the ophiolite (Fig. 1;Lisenbee, 1972; Monod et al., 1991; Okay et al., 1998; Önen and Hall, 1993; Önen, 2003; Plunder et al., 2013). Sub-ophiolitic metamorphic soles typically form during the initiation of intra-oceanic subductions when cold oceanic crust is buried in thermally immature subduction zone and brought in contact with hot mantle (Hacker, 1990; Parrot and Whitechurch, 1978; Woodcock and Robertson, 1977). Metamorphic soles exhibit an upward increase of the metamorphic grade, reaching in the Tavşanlı Zone the amphibolite-facies paragenesis hornblende–plagioclase ± garnet ± epidote ± rutile ± quartz for which climax PT conditions lie at 8.5 ± 3.5 kbar and ~ 700 °C (Okay et al., 1998; Önen and Hall, 2000). K/Ar and Ar/Ar cooling ages of amphiboles from the metamorphic sole range from 87.9 ± 5.2 to 101 ± 3.8 Ma (Harris et al., 1994; Önen, 2003) with two Ar/Ar cooling ages of 93.0 ± 2 and 90.0 ± 3 Ma (Önen, 2003). In several localities of the Tavşanlı zone and other regions, the HT metamorphic-sole paragenesis exhibits a HP–LT overprint (Dilek and Whitney, 1997; Okay et al., 1998; Önen and Hall, 2003). In the Tavşanlı zone, the amphibolite-facies association is overgrown by a blueschist paragenesis of lawsonite + sodic amphibole ± sodic pyroxene for which conditions were estimated at 300 °C and at least 5 kbar (Okay et al., 1998; Önen and Hall, 2000; Plunder et al., 2013).

(2) The Cretaceous accretionary complex is tectonically sandwiched between the ophiolite and HP–LT metamorphosed continental rocks (Fig. 1). It is made of imbricated slices (i.e. it does not correspond to a block-in-matrix structure) of weakly metamorphosed, offscrapped oceanic material (radiolarian cherts, basalts, pillow lavas, tuffs). It was first described by Kaya (1972) and Lisenbee (1972) south of Tavşanlı and in the Orhaneli region, respectively (Fig. 1). Palaeontological studies of the radiolarians yielded late Triassic to Late Cretaceous ages, supporting the idea that the complex results from the closure of a Mesozoic, Neotethyan oceanic realm (Bragin and Tekin, 1996; Göncüoglu et al., 2006; Okay et al., 2012; Servais, 1981; Tekin and Göncüoglu, 2009; Tekin et al., 2002). Based on mineral assemblages and structural data, Plunder et al. (2013) divided the accretionary complex into two units: a lower oceanic complex (hereafter OC2) affected by blueschist-facies metamorphism (Fe–Mg-carpholite in tiny pelitic layers found in meta-cherts and lawsonite–sodic pyroxene–glaucophane in meta-mafic rocks) with PT conditions of 10–15 kbar and 300–400 °C corresponding to 100-metre thick slices. The upper unit (hereafter OC1) consists of incipient to sub-blueschist-facies metamorphic rocks with formation conditions of 4–8 kbar and ~200 °C and has a thickness of up to one kilometre (Okay, 1982, 1986; Topuz et al., 2006; this study).

(3) The Orhaneli sequence lies below the accretionary complexes, or directly below the ultra-mafic thrust sheet in the absence of the former. It consists of a coherent stratigraphic sequence of, from top to bottom, metabasite, marble and metaclastic rocks, known as the Devlez, İnönü and Kocasu formations, respectively (Lisenbee, 1972; Okay, 1980a, 1980b, 1986; Okay and Kelley, 1994; Servais, 1981). The Devlez formation is composed of blueschist-facies metabasite, metachert, and metatuff with a thickness of one kilometre (Okay, 1980a, 1980b; van der Kaaden, 1966), for which no PT estimates are available. In this formation, HP–LT metamorphism was dated at 78.5 ± 1.6 and 79.7 ± 1.6 Ma using Rb/Sr isochrons including phengite

Table 1
Mineral occurrence for selected samples. x, present phase; o, secondary phases. Mineral abbreviations after Kretz (1983). Op: opaque mineral. Additional symbol explained in Fig. 2.

		Mineral													GPS coordinate	
Sample	unit	Qtz	Phg	Cpx	Car	Cld	Lws	Ep	Gln	Grt	Chl	Spn	Rt	Other	N (°,′,″)	E (°,′,″)
11OR33	metam. sole	x						x		x	o	x	x	Hbl - Ab - Ap	39°47′43.1″	28°41′13.4″
11TAV13a	metam. sole						o		o	x				Hbl	39°28′15.7″	29°31′59.8″
11TAV13b	metam. sole	x	x	Na-Px			x		o	x				Ab	39°28′15.7″	29°31′59.8″
DU1206	metam. sole	x	x				o		o	x	o	x	x		39°41′2.50″	29°19′36.9″
KO1218	metam. sole			x			o	x	o	x	o	x	x	Ilm	39°54′25,2″	28°48′24,4″
OR1028a	metam. sole	x	x				o		o	x	o	x	x	Hbl	39°41′9.4″	29°19′3.9″
TAV1008a	metam. sole	x		Na-Px			o		o	x		x		Ab	39°28′15.7″	29°31′59,8″
KO1205	OC1			Aug						x	x			Plg - Pmp - glass	39°51′13.8″	28°35′17.8″
11OR16a	OC2	x	x		x						x		x		39°43′33.3″	28°40′46.3″
11OR16b	OC2	x		x			x		x		x	x		Ap	39°43′33.3″	28°40′46.3″
DE1201c	OC2	x	x		x		x				x		x		39°42′16.1″	29°46′3.8″
DE1202b	OC2			x			x	x	x		x	x			39°42′16.1″	29°46′3.8″
DE1202c	OC2			x			x		x		x	x			39°42′14″	29°46′15.4″
DU1215	OC2	x	x		x		x				x		x	Ap	39°38′50″	29°4′49.6″
DU1216	OC2	x	x		x						x		x	Ap	39°40′37.9″	29°4′16.5″
KO1213	OC2	x	x		x						x		x		39°43′29.5″	28°40′48.4″
11TAV20	Devlez / OC3	x	x				x	x	x	x		x	x	Aln	39°45′34″	29°50′27.2″
11TAV23	Devlez / OC3	x		x			x	x	x	x				Op	39°49′44.5″	29°33′12.3″
11TAV31	Devlez / OC3	x	x	x			x		x		x	x			39°47′43″	29°57′25.9″
TAV1004	Devlez / OC3	x	x				x		x	x	x			Op	39°45′41.8″	29°49′49,1″
TAV1110a	Devlez / OC3			Aug			x		x		x	x			39°45′37.7″	29°47′44″
TAV1110b	Devlez / OC3			Aug + Na-Px			x		x		x	x		Pmp	39°45′37.7″	29°47′44″
11DU04	Kocasu	x	x	x			x				o				39°42′02.0″	29°17′24.8″
11OR22	Kocasu	x	x	x		x			x		x				39°47′43.1″	28°41′13.4″
11TAV07a	Kocasu	x	x			x	x				x			Ap	39°39′03.3″	28°24′37.6″
OR1006	Kocasu	x	x	x		x	x		x		o		x		39°53′48.6″	29°01′19.9″
OR1012	Kocasu	x	x	x		x	x		x		o		x		39°55′05.5″	29°10′45.4″
OR1013b	Kocasu	x	x	x		x	x		x		o			Ap	39°55′05.5″	29°10′37.4″
OR1024	Kocasu	x	x	x		x	x		x				x	Tur	39°52′52.4″	29°05′36.5″

(Sherlock et al., 1999). At the base of the Devlez formation, a 5- to 10-metre thick calcschist level was observed, and corresponds to the transition with the İnönü formation in the Devlez area (Okay, 1980a, 1980b). The İnönü Marble (Servais, 1981) is considered to range from the upper Triassic to the upper Cretaceous in depositional age on the basis of the presence of Norian conodonts (Kaya et al., 2001) and the comparison with the Tauride carbonate-platform series (Gutnic et al., 1979). The İnönü Formation consists of interlayered impure, phengite-bearing marly marble and chert that pass downwards to massive white to grey marble at the base (Okay, 1986; Servais, 1981). Its thickness varies from 1 to 3 kilometre (Okay, 1986). The İnönü formation passes gradually to the underlying Kocasu formation, as observed in the Orhaneli region (Lisenbee, 1972). The Kocasu formation consists of a 1-km thick sequence of quartz-rich greyschists (i.e., graphite-rich mica schists) and white phengite-rich schists (Lisenbee, 1972; Okay, 2002; Okay and Kelley, 1994). The depositional age of the formation is poorly known but must be post Permo-Carboniferous because it contains detrital zircons with magmatic ages of 310–283 Ma (U/Pb; Okay et al., 2008). The PT conditions for the high-pressure assemblage in the Kocasu Formation were estimated at 22 ± 4 kbar and 430 ± 30 °C (Okay, 2002; Okay and Kelley, 1994). Maximum-temperature estimates obtained by Raman spectroscopy on carbonaceous matter (RSCM, Beyssac et al., 2002) yield T_{max} of ~470–550 °C (Plunder et al., 2013). The Ar/Ar ages on phengite from these rocks range from 70 to 123 Ma (Okay and Kelley, 1994; Okay et al., 1998; Sherlock et al., 1999). This large spread was attributed to excess argon during the HP-LT event (Sherlock et al., 1999; Sherlock and Kelley, 2002;) and the age of metamorphism is regarded as ~80 ± 5 Ma on the basis of Rb/Sr data (Sherlock et al., 1999).

3. Sampling, analytical techniques and methods

The studied samples, all from the Tavşanlı Zone, were collected in the Orhaneli unit, the accretionary complexes (both OC1 and OC2), and the sub-ophiolitic metamorphic sole. The collection comprises metapelitic (pelitic schists, sodic metapelites) and metabasic (basalts, tuffs, pillow breccias) rocks. Out of >250 samples cut in the XZ plane of deformation, 30 representative ones were selected for chemical analysis, Raman spectroscopy and thermobarometric calculations. Mineral assemblages for samples mentioned in the text are given in Table 1.

Electron-microprobe analyses were carried out at CAMPARIS (University Paris 6) using SX50, SX100 and SX Five instruments. Classical analytical conditions were adopted (15 kV acceleration voltage, 10 nA beam current, 2–3 μm beam size, wavelength-dispersive spectroscopy mode). Albite (Na), diopside (Mg, Si, Ca), orthoclase (Al, K), $MnTiO_3$, Fe_2O_3 (Fe) and Cr_2O_3 (Cr) were used as standards for the relevant elements. Additional observations were made using a Zeiss Σigma scanning electron microscope (SEM) at Laboratoire de Géologie, Ecole Normale Supérieure (ENS), Paris.

Table 2
Whole-rock compositions used for PT estimates. Bulk compositions were obtained by chemical analysis at IPG Strasbourg (oxide wt.%) or by scanning electron microscope image analysis (at %).

Sample – % wt ox	SiO2	TiO2	Al2O3	FeO	MnO	MgO	CaO	Na2O	K2O	P2O5
11OR16	68.97	0.64	13.98	6.39	0.80	3.10	0.10	0.59	0.50	0.07
OR1006b	75.70	0.52	10.60	4.36	0.04	0.85	1.15	1.69	1.89	0.04
OR1024	55.76	1.01	20.72	8.67	0.06	2.49	0.58	1.83	3.20	n.a.
OR1012	55.60	1.14	20.80	7.62	0.08	2.57	0.24	2.07	4.02	0.12
KO1218	47.50	2.82	13.10	15.40	0.18	5.44	8.70	2.94	0.99	1.75
11TAV31	45.70	1.30	17.00	10.10	0.15	4.18	11.10	2.91	1.00	0.25
Sample – at %	Si	Ti	Al	Fe	Mn	Mg	Ca	Na	K	P
11OR22	60.35	0.67	18.29	5.37	0.07	2.49	0.53	3.43	3.51	0.15
DU1215	30.46	n.a.	2.02	0.69	0.03	0.70	0.32	n.a.	0.11	n.a.
KO1213	74.57	n.a.	16.16	3.71	0.50	5.26	n.a.	n.a.	0.30	n.a.
DE1201c	94.94	0.15	21.198	6.77	0.60	5.75	1.02	n.a.	0.45	n.a.

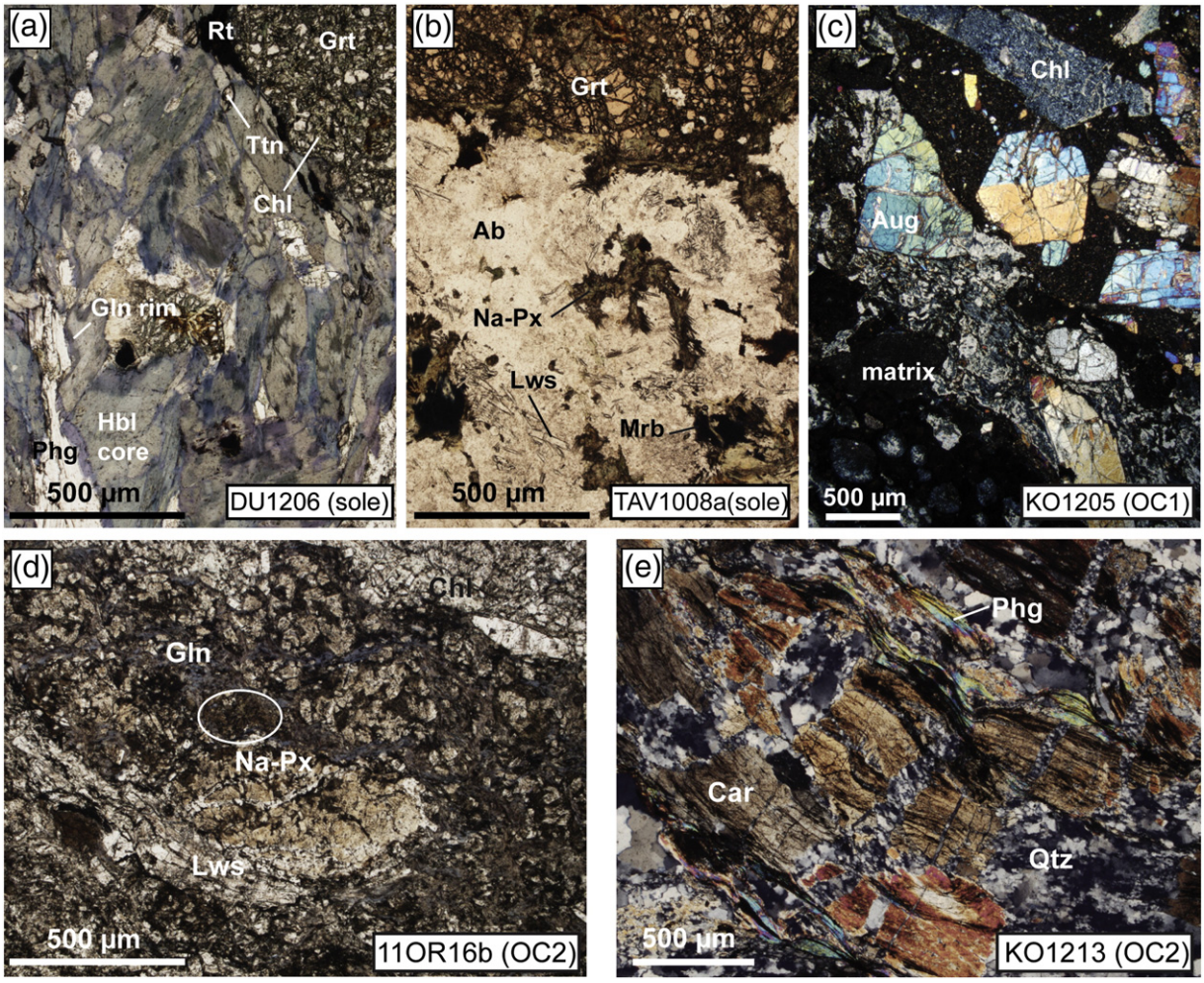

Fig. 2. Photomicrograph of selected samples from the metamorphic sole and OC1 and OC2 units. (a) Metamorphic sole from Elmaağacı showing initial Hbl + Grt + Rt paragenesis and the high-pressure overprint. Plane-polarised light (PPL); (b) Plagiogranite in the metamorphic sole south of Tavşanlı showing high-pressure overprint with the development of Lws, Na-Px and Mrb (PPL); (c) Typical pillow-breccia from OC1 with pristine augite. Cross-polarised light (XPL); (d) Blueschist-facies metabasite from OC2 with the typical paragenesis Gln + Lws + Na-Px ± Chl (PPL); (e) Carpholite-bearing sample from OC2 corresponding to the same location as picture (d) (XPL). All abbreviations from Kretz (1983) except for Car, carpholite; Na-Px, sodic pyroxene; Phg, phengite.

Raman spectra on carbonaceous material were obtained using a Renishaw inVia Spectrometer at Laboratoire de Géologie, ENS, and part of them come from the study by Plunder et al. (2013). A 514 nm argon laser in circular polarisation was used. The laser was focused on polished thin section using a Leica microscope with a 100× objective. Laser power was set at ~2-4 mW. Carbonaceous matter was analysed below a transparent mineral, generally quartz or jadeite. Between 10 and 25 spectra per sample were acquired in the extended scanning mode 1000–2000 cm^{-1} with an acquisition time of 30 to 60 s and 1–3 accumulations, using the calibration method of Beyssac et al. (2002, 2003). Spectra were then processed following the procedure described by Beyssac et al. (2002). This thermometer allows an accuracy of ± 50 °C in the range of 350–650 °C (Beyssac et al., 2002).

The PT pseudosections (i.e. phase diagram for a fixed bulk composition) were calculated using the Gibbs-free-energy minimization procedure of de Capitani and Brown (1987) with the software THERIAK/DOMINO (de Capitani and Petrakakis, 2010) and the databases of Holland and Powell (1998) or Berman (1988) updated with new data (tcdb55cc2d.bs and Jun92.bs respectively in the THERIAK/DOMINO package).

Whole-rock compositions were obtained for ten samples. Six were analysed for major and trace elements at IPG Strasbourg (Table 2). The other compositions were estimated from EMP mineral analyses and modal proportions determined by image analysis, or directly by image analysis using the SEM (Table 2).

4. Petrography

4.1. Subduction initiation remnants: metamorphic sole

The top part of the metamorphic sole consists of amphibolite-facies rocks. The dominant mineral assemblage in metabasite of the Orhaneli region is hornblende (up to 70%) + plagioclase + epidote + rutile + quartz ± garnet ± opaque, as reported by Okay et al. (1998). Clinopyroxene was occasionally found as inclusion in ilmenite in one sample (KO1218, Çivili area). In this sample, ilmenite shows lamellar development and overgrowth of titanite. Rutile was found as inclusion in garnet, amphibole or titanite. Titanite is found as euhedral crystals growing in the green amphibole matrix (Fig. 2a), included in amphibole or garnet. Epidote is present in some samples, coexisting with hornblende, and as inclusion in garnet (11OR33). White mica can be observed in some samples, coexisting with amphibole, garnet or former plagioclase (OR1028a). As already noticed by Okay et al. (1998), blue amphibole rims developed around hornblende, and lawsonite is found coexisting with albite as products of plagioclase replacement. This overprint is better observed in the region of El Maağacı, and south of Tavşanlı (DU1206, TAV1008a; Fig. 2a,b).

South of Tavşanlı, in a sample (TAV1008a; Fig. 2b) exhibiting a fine-grained (magmatic) structure, lawsonite and albite were found replacing plagioclase. This sample also contains garnet, riebeckite and sodic

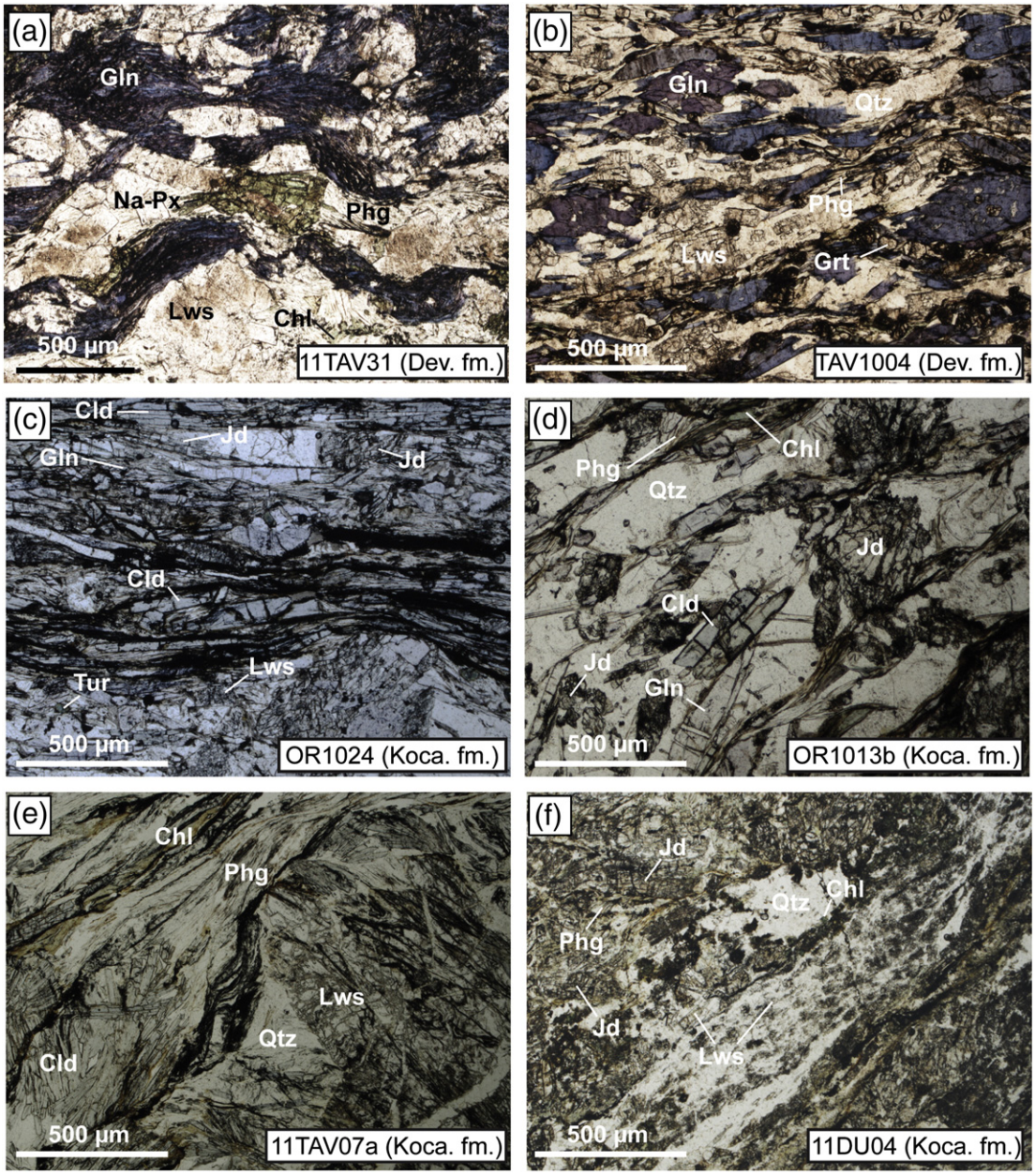

Fig. 3. Photomicrograph of selected samples from Devlez and Kocasu formations. (a) Blueschist-facies metabasite; (b) Blueschist-facies metachert; (c) Typical greyschist of the Orhaneli area with the well-preserved Jd + Gln + Cld + Lws paragenesis (PPL); (d) Greyschist from the Orhaneli region with the paragenesis Jd + Gln + Cld (PPL); (e) Lws + Cld-bearing greyschist from the region of Dursunbey (PPL); (f) Jd + Lws-bearing greyschist from the region of Elmaağacı (PPL).

pyroxene (which grew statically or as vein fillings). This very light coloured sample is rich in plagioclase (up to 70%) and differs from the typical metabasite. It will be referred to as the white metamorphic sole below, and may represent a metamorphosed plagiogranite.

4.2. Oceanic subduction remnants: accretionary complexes OC1 and OC2

In OC1, basalts have preserved their magmatic texture, with large pristine clinopyroxene phenocrysts (KO1205; Fig. 2c). Augite occasionally was turned into sodic pyroxene by static replacement. Albitised plagioclase is common as observed by Okay (1982). Most of the matrix is made of aggregates of chlorite and phases such as pumpellyite and occasionally very fine-grained lawsonite.

Metabasites from OC2 contain blueschist-facies assemblages with lawsonite, sodic amphibole, sodic pyroxene, and chlorite (11OR16; Fig. 2d). Minor quartz, titanite, white mica, and carbonate might also be observed. Sodic pyroxene is as abundant as sodic amphibole as noticed for the lawsonite zone of the Devlez formation (Okay, 1980a, 1980b). Carpholite-bearing rocks (i.e., thin metapelitic layers in metacherts) are typically interbedded with metabasites and carpholite is present as truncated fibres growing along the foliation plane (KO1213; Fig. 2e). Carpholite coexists with predominant quartz (up to 70% of the mode), white mica, chlorite, and occasionally lawsonite (DU1216).

4.3. Continental subduction remnants: Orhaneli unit

- Devlez formation: The petrography of the Devlez formation was largely described by Okay (1980a, 1980b). About 75 metabasite and metachert additional samples were collected. Metabasites consist up to 80% of lawsonite and sodic amphiboles at textural equilibrium, the rest being sodic pyroxene, white mica, chlorite, titanite, quartz, albite, opaque, or carbonate (11TAV31; Fig. 3a). The proportion of sodic pyroxene varies significantly from sample to sample

(5–25%). All above mentionned phases present textural equilibrium. Epidote can be found in metabasite samples, as inclusions in lawsonite or garnet (11TAV20). Metacherts show garnet ± sodic amphibole ± lawsonite ± white mica ± opaque (haematite) assemblages (TAV1004; Fig. 3b). Rare sodic pyroxene or epidote were also found in those rocks (11TAV23). The sample used hereafter for thermodynamic modelling (11TAV31) is a metabasite made of lawsonite (~30–40%), sodic amphibole (~25–35%), sodic pyroxene (~10–20%) and white mica (~5–10%). Chlorite, titanite, and quartz are also present as minor phases, constitutiong less than 5% of the mode. Foliation is well defined by sodic amphibole with an intense dark blue pleochroism, characteristic of Fe^{3+} end-members (Fig. 3a). Sodic pyroxene is green, slightly pleochroic, prismatic and does not replace a former magmatic pyroxene. It coexists with both lawsonite and sodic amphibole. Lawsonite forms typical rectangular-shaped crystals, with fine-grained inclusions. White mica flakes are found either parallel to the foliation or crystallised statically. Carbonate veins were observed crosscutting the main foliation.

- Kocasu formation: About 100 samples from the Kocasu formation were collected in the greyschists of the Orhaneli, Kocasu, Dursunbey, Tekerler, Köseler regions and were petrographically studied. The petrography of the greyschist was described in the literature and the reader is refered to Okay and Kelly (1994) and Okay (2002) for more details. Commonly observed minerals are quartz, white mica, jadeite, chloritoid, sodic amphibole, lawsonite, and chlorite (OR1024, OR1013b, 11TAV07a, 11DU04; Fig. 3c,d,e,f). Sodic amphibole will be referred to as glaucophane for the Kocasu formation. Minor rutile, albite, tourmaline, carbonaceous matter, carbonates and apatite were also observed. Regardless of the sampling area, greyschists are made of white mica and quartz as major phases, generally forming more than 50% of the mode. In most samples, foliation is well defined by white mica and occasionally chlorite, or brown oxychlorite. Chlorite commonly crystallises from both chloritoid and glaucophane or in late shear bands, and so represents retrograde stages. Jadeite mainly occurs as prismatic crystals up to 0.5 mm in size (Fig. 3c,d,f), but reach up to 2–3 mm in size in some restricted areas (in Orhaneli region, near Kabaklar village). It can be found as pristine crystals (Fig. 3c,d), some of which contain abundant carbonaceous matter or other mineral inclusions (Fig. 3f). Glaucophane is found as elongated crystals, free of inclusions (Fig. 3c,d) and occasionally zoned, cores being more coloured than rims in plane-polarised light. It can be found included in jadeite. As suggested by Okay (2002), the close proximity of listed

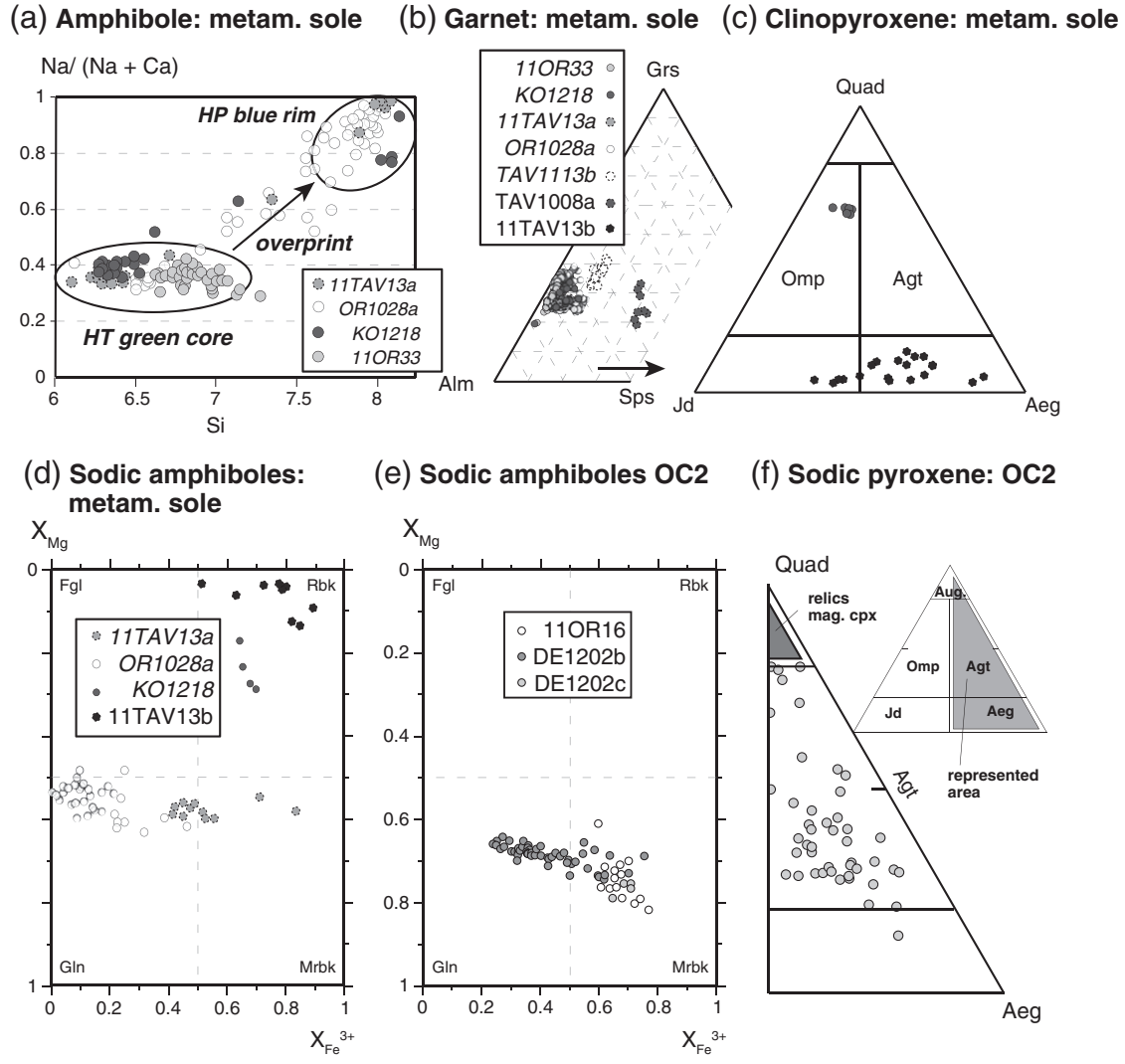

Fig. 4. Representative microprobe analyses for samples of the metamorphic sole and of metabasite from OC2 unit. (a) Amphibole; (b) Garnet; (c) Clinopyroxene; (d) and (e) Sodic amphibole; (f) Sodic pyroxene. On all figures sample numbers in italics refer to metabasite, those in normal font to metasediments. Additional abbreviations, Quad, Ca-Fe-Mg clinopyroxene; Aeg, Aegirine; Fgl, ferro-glaucophane.

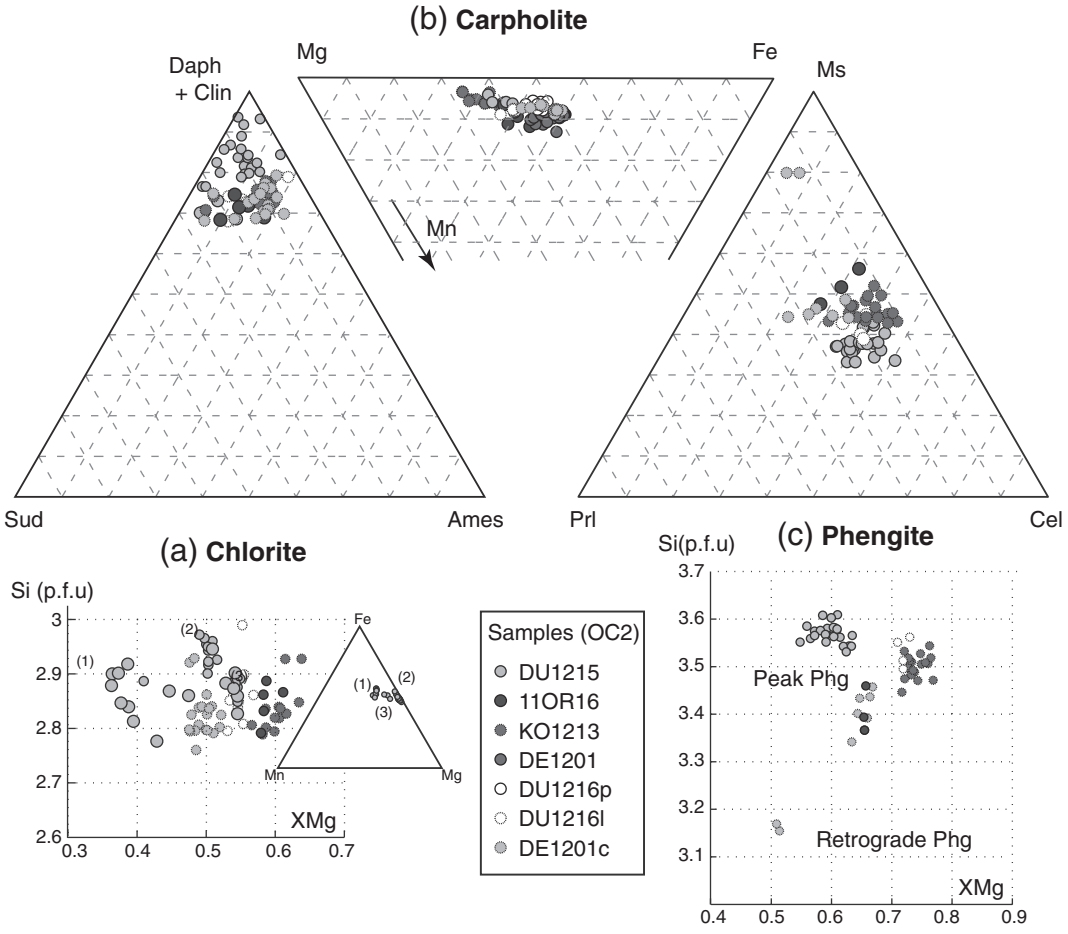

Fig. 5. Representative microprobe analyses from carpholite-bearing samples of OC2. (a) Chlorite; (b) Carpholite; (c) Phengite. For phengite and carpholite part of the analyses comes from Plunder et al. (2013). Additional abbreviations : Daph, daphnite ; Clin, clinochlore; Ames, amesite; Sud, sudoite; Cel, celadonite.

minerals, textural equilibrium evidence and the absence of textural reaction (Fig. 3c,d,e,f) allow the assumption of equilibrium for this rather uncommon assemblage. This is particularly clear in sample OR1024 (Fig. 3c).

5. Mineral composition

This section reports the typical mineral compositions for samples of the metamorphic sole, the accretionary complex OC2, and the Orhaneli sequence. Some representative analyses are plotted on Figs. 4, 5 and 6 and given in Table 3.

5.1. Metamorphic sole rocks

5.1.1. Plagioclase

Plagioclase in metabasite or in the white metamorphic sole is entirely pseudomorphed by albite and lawsonite through the general reaction plagioclase + H_2O = lawsonite + albite. Considering the observed modal amounts of lawsonite and albite, and the fact that the measured anorthite content in albite is < An_{10}, we estimate that plagioclase composition was originally $An_{20\text{-}40}$.

5.1.2. Amphibole

Amphibole nomenclature follows the classification of Leake et al. (1997). Amphibole formula unit were calculated on 23 oxygenes and Fe^{3+}/Fe^{2+} was estimated assuming a total sum of 13 cations. In metabasite, amphibole cores have a typical composition between pargasite and hornblende (Fig. 4a). The X_{Mg} ratio [with $X_{Mg} = Mg/(Mg + Fe^{2+})$] varies between localities from 0.30 to 0.60 (11TAV13a, OR1028a, KO1218, 11OR33). In contrast, rims are of glaucophane or riebeckite compositions (Fig. 4a), with X_{Mg} and X^{3+}_{Fe} values varying from one sample to another (Fig. 4d). In the white metamorphic sole all measured amphibole have a riebeckite composition (11TAV13b; Fig. 4d).

5.1.3. Garnet

Garnet composition analysed in the metabasite is mostly between almandine and grossular: $Alm_{55\text{-}65}$-$Grs_{20\text{-}30}$-$Sps_{0.01\text{-}0.06}Prp_{0.1}$ (Fig. 4b). Rims generally have the highest grossular contents and pyrope content is constant. Garnet analysed in the white metamorphic sole have a higher content in spessartine (TAV1008a; Fig. 4b).

5.1.4. Pyroxene

The Fe^{3+} content in pyroxene was estimated using the generic formula of Droop (1987). Two samples containing clinopyroxene were analysed (Fig. 4c). In sample KO1218 pyroxene has an omphacite composition, with the following composition $Jd_{22}Quad_{64}Aeg_{14}$ (Fig. 4c; Table 3). It is assumed to represent high-temperature conditions, as it is included in ilmenite, coexisting with garnet, Ca-amphibole and plagioclase. Clinopyroxene compositions in the white metamorphic sole are low in Ca, high in Na (>0.8 pfu) and with variable Fe^{3+}. These compositions are related to the HP overprint as attested by the coexistence with sodic amphibole and lawsonite.

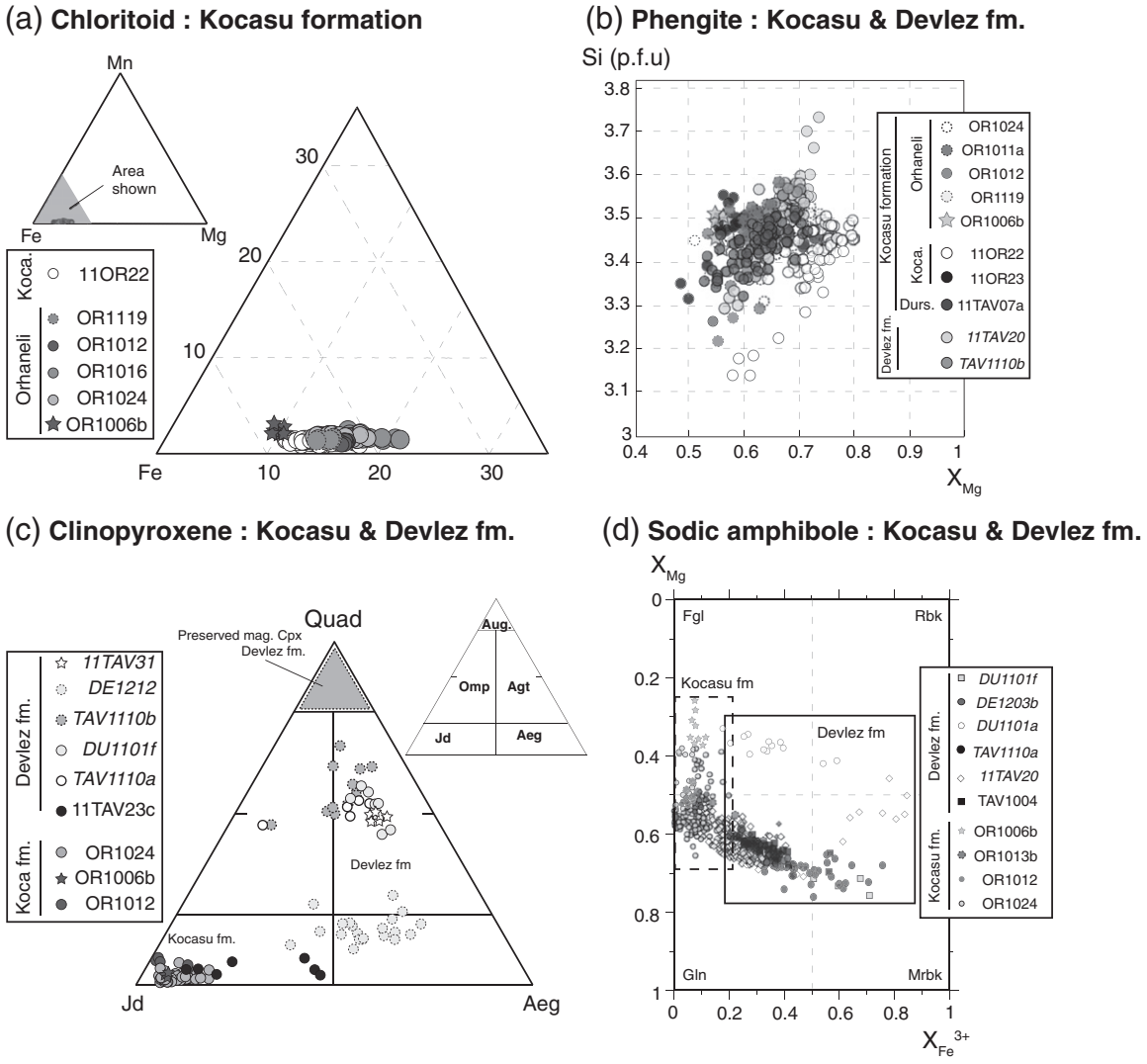

Fig. 6. Representative microprobe analyses for samples of the Devlez and Kocasu formations. (a) Chloritoid; (b) Phengite; (c) Clinopyroxene; (d) Sodic amphibole. Data are the same as in Plunder et al. (2013).

5.2. Oceanic complex (OC2) rocks

5.2.1. Sodic amphibole

In the metabasite sodic amphiboles analysed are Fe^{3+}-rich glaucophane to magnesio-riebeckite with X^{3+}_{Fe} [$= Fe^{3+} / (Fe^{3+} + Al^{3+})$] in the range 0.2–0.8, and X_{Mg} within the range 0.6–0.8 (11OR16, DE1202b, DE1202c; Fig. 4e; Table 3). Amphibole cores occasionally have a composition close to barroisite. Noteworthily, epidote crystals with about 0.75 Fe^{3+} per 3 Si formula unit were observed as inclusions in sodic amphibole.

5.2.2. Sodic pyroxene

Sodic pyroxene in metabasite generally has a composition of aegirine-augite in this unit (DE1202c; Fig. 4f), and some cores still are augitic. Sodic pyroxene displays strong variations in composition but no systematic zoning was observed.

5.2.3. Chlorite

Chlorite was measured only in carpholite-bearing rocks of OC2. When present, it coexists with carpholite, quartz and phengite. The X_{Mg} value ranges from 0.4 to 0.6 (Fig. 5a). Chlorite with the lowest X_{Mg} was found in sample DU1215, and is Mn-rich (Fig. 5a). Si contents range between 2.8 to 3.0 p.f.u. (per formula unit; Fig. 5a; Table 3) and typical composition is close to clinochlore + daphnite, with $X_{Clinochlore} + X_{Daphnite} > 0.65$ (following the classification of Vidal and Parra, 2000).

5.2.4. Carpholite

Pristine Fe–Mg-carpholite was observed in few samples from the OC2, as reported by Plunder et al. (2013) (Fig. 1). It coexists at the scale of the outcrop with rocks containing glaucophane, lawsonite, and sodic pyroxene (11OR16b). Carpholite X_{Mg} [with $X_{Mg} = Mg/(Mg + Fe^{2+})$] varies in the range 0.45 to 0.60 with constantly low Mn contents (<0.1 p.f.u.) (Fig. 5b). The Fe^{3+} content is consistently lower than 0.1 p.f.u. (Table 3), it was calculated as (2 – Al) and Fe^{2+} content as $Fe^{tot} - Fe^{3+}$, following Goffé and Oberhänsli (1992).

5.2.5. Phengite

In carpholite-bearing rocks the Si content p.f.u. ranges from 3.15 to 3.6 due to the Tschermak substitution $[2Al^{3+} = Si^{4+} + (Fe,Mg)^{2+}]$ and the pyrophyllitic substitution $[Al^{3+} + K^{+} = Si^{4+}]$ (Fig. 5c). The K content is between 0.7 and 0.9 p.f.u. (Fig. 5c; Table 3). The mole fraction of paragonite, $X_{Paragonite}$ [Na/(Na + K))] is always lower than 0.1. Phengite composition shows virtually no intra-sample variations and ranges between $0.4 < X_{Celadonite} < 0.7$ and $0.1 < X_{Pyrophyllite} < 0.3$ except for sample DE1201c where phengite close to muscovite composition

Table 3
Selected representative EPMA analyses for phengite, chloritoid, sodic amphibole, clinopyroxene, carpholite and lawsonite.

Mineral	phg								
Sample	OR1024	or1006b	OR1012	11OR22	11tav31	de1201c	ko1213	du1215	11OR16
Analyse	1	54	165	163	25	37	155	20	79
SiO2	51.76	51.26	51.19	52.11	51.60	51.26	50.75	53.03	48.89
TiO2	0.16	0.11	0.12	0.06	0.03	0.52	0.06	0.26	0.52
Al2O3	25.56	25.53	25.24	26.47	22.82	24.99	26.35	23.16	25.21
Cr2O3	0.06	0.00	0.01	0.00	0.04	0.09	0.02	0.00	0.05
FeO	3.05	3.80	3.28	2.26	5.00	3.75	2.48	4.59	3.84
MnO	0.00	0.00	0.07	0.06	0.06	0.15	0.04	0.47	0.06
MgO	3.54	2.79	3.65	3.59	4.38	4.25	3.51	3.56	4.04
CaO	0.01	0.11	0.06	0.00	0.06	0.15	0.00	0.11	0.05
Na2O	0.16	0.18	0.26	0.08	0.05	0.08	0.18	0.05	0.14
K2O	10.49	9.76	10.18	10.08	10.36	9.06	10.07	9.62	9.27
Sum	94.77	93.54	94.04	94.72	94.40	94.30	93.45	94.84	92.07
Formula unit									
Si	3.48	3.49	3.47	3.48	3.52	3.46	3.44	3.57	3.39
Ti	0.01	0.01	0.01	0.00	0.00	0.03	0.00	0.01	0.03
Al	2.03	2.05	2.02	2.08	1.84	1.99	2.11	1.84	2.06
Cr	0.00	0.00	0.00	0.00	0.00	0.01	0.00	0.00	0.00
Fetot	0.17	0.22	0.19	0.13	0.29	0.21	0.14	0.26	0.22
Fe3									
Fe2									
Mn	0.00	0.00	0.00	0.00	0.00	0.01	0.00	0.03	0.00
Mg	0.35	0.28	0.37	0.36	0.45	0.43	0.36	0.36	0.42
Ca	0.00	0.01	0.00	0.00	0.00	0.01	0.00	0.01	0.00
Na	0.02	0.02	0.03	0.01	0.01	0.01	0.02	0.01	0.02
K	0.90	0.85	0.88	0.86	0.90	0.78	0.87	0.83	0.82

Mineral	cld			
Sample	OR1024	11or22	or1012	or1006b
Analyse	144	52	18	17
SiO2	23.39	23.93	24.69	23.83
TiO2	0.09	0.02	0.10	0.03
Al2O3	39.01	40.77	39.07	39.83
Cr2O3	0.07	0.02	0.00	0.00
FeO	24.67	23.65	23.78	26.42
MnO	0.57	0.50	0.47	0.44
MgO	2.81	2.53	2.48	1.48
CaO	0.00	0.03	0.03	0.03
Na2O	0.02	0.02	0.03	0.00
K2O	0.04	0.00	0.03	0.01
Sum	90.66	91.45	90.68	92.07
Formula unit				
Si	1.99	1.99	2.08	2.00
Ti	0.01	0.00	0.01	0.00
Al	3.91	4.00	3.87	3.94
Cr	0.01	0.00	0.00	0.00
Fetot	1.75	1.65	1.67	1.86
Fe3				
Fe2				
Mn	0.04	0.04	0.03	0.03
Mg	0.36	0.31	0.31	0.19
Ca	0.00	0.00	0.00	0.00
Na	0.00	0.00	0.01	0.00
K	0.00	0.00	0.00	0.00
XMg	0.17	0.16	0.16	0.09

Mineral	Na-amph				
Sample	OR1024	or1006b	OR1012	11tav31	11tav31
Analyse	5 / 1 .	b40	5.00	82/1.	82/1.
SiO2	58.73	55.78	58.07	56.74	56.29
TiO2	0.00	0.09	0.13	0.00	0.06
Al2O3	12.18	11.08	10.66	4.08	4.58
Cr2O3	0.00		0.00	0.02	0.01
FeO	12.11	19.13	14.20	19.17	19.49
MnO	0.06	0.00	0.01	0.41	0.35
MgO	8.06	3.85	6.97	9.37	9.14
CaO	0.03	0.15	0.07	1.38	1.29
Na2O	7.03	6.30	6.37	6.06	6.08
K2O	0.00	0.00	0.00	0.02	0.02
Sum	98.20	96.38	96.49	97.27	97.31
Formula unit					
Si	8.01	8.00	8.12	8.03	7.96
Ti	0.00	0.01	0.01	0.00	0.01
Al	1.96	1.87	1.76	0.68	0.76
Cr	0.00	0.00	0.00	0.00	0.00
Fetot					
Fe3	0.15	0.31	0.24	1.18	1.25
Fe2	1.23	1.98	1.42	1.09	1.05
Mn	0.01	0.00	0.00	0.05	0.04
Mg	1.64	0.82	1.45	1.98	1.93
Ca	0.00	0.02	0.01	0.21	0.20
Na	1.86	1.75	1.73	1.66	1.67
K	0.00	0.00	0.00	0.00	0.00
XMg	0.57	0.29	0.51	0.65	0.65
XFe3	0.07	0.14	0.12	0.63	0.63

Mineral	cpx				
Sample	or1024	or1012	or1012	11tav31	11tav31
Analyse	119	78	79	45	11
SiO2	59.63	58.50	58.96	52.26	54.26
TiO2	0.07	0.09	0.09	0.04	0.07
Al2O3	23.03	21.97	22.79	4.40	3.19
Cr2O3	0.01	0.02	0.04	0.41	0.24
FeO	3.06	3.76	3.63	17.18	19.72
MnO	0.00	0.01	0.11	0.43	0.30
MgO	0.22	0.25	0.12	5.09	4.60
CaO	0.37	0.40	0.21	9.20	8.26
Na2O	14.46	14.03	14.35	7.03	8.74
K2O	0.02	0.00	0.01	0.98	0.04
Sum	100.86	99.04	100.31	97.02	99.41
Formula unit					
Si	2.02	2.02	2.01	1.99	2.02
Ti	0.00	0.00	0.00	0.00	0.00
Al					
Cr	0.92	0.90	0.92	0.19	0.14
Fetot					
Fe3	0.00	0.00	0.01	0.37	0.45
Fe2	0.09	0.11	0.10	0.18	0.16
Mn	0.00	0.00	0.00	0.01	0.01
Mg	0.01	0.01	0.01	0.29	0.25
Ca	0.01	0.02	0.01	0.38	0.33
Na	0.95	0.94	0.95	0.52	0.63
K	0.00	0.00	0.00	0.05	0.00

Mineral	car				
Sample	DU1215	11OR16	11OR16	KO1213	De1201c
Analyse	7 / 1 ,	5	6	111	47
SiO2	37.59	37.81	37.70	38.20	37.23
TiO2	0.71	0.25	0.24	0.51	0.41
Al2O3	30.87	31.40	30.99	31.57	30.51
Cr2O3	na	0.12	0.07	0.06	0.00
FeO	10.49	9.69	9.95	9.69	11.74
MnO	1.18	1.75	1.38	1.42	1.44
MgO	7.08	6.15	6.63	6.70	5.47
CaO	0.00	0.01	0.01	0.00	0.00
Na2O	0.03	0.00	0.02	0.00	0.00
K2O	0.06	0.02	0.02	0.00	0.01
Sum	88.01	87.19	87.00	88.16	86.81

Mineral	lws			
Sample	DU1215	DU1215	De1201c	De1201c
Analyse	34 / 1 ,	47 / 1 ,	16	17
SiO2	38.29	37.76	39.02	38.76
TiO2	0.20	0.25	0.06	0.01
Al2O3	31.23	31.02	31.59	31.73
Cr2O3	na	na	na	na
FeO	1.38	1.05	0.63	0.78
MnO	0.13	0.09	0.04	0.11
MgO	0.00	0.00	0.00	0.00
CaO	16.91	16.90	16.82	17.26
Na2O	0.00	0.00	0.00	0.00
K2O	0.00	0.00	0.00	0.00
Sum	88.14	87.07	88.17	88.65

Table 3 (*continued*)

Mineral	car					Mineral	lws			
Formula unit						Formula unit				
Si	1.99	2.01	2.01	2.01	2.01	Si	2.02	2.02	2.05	2.03
Ti	0.03	0.01	0.01	0.02	0.02	Ti	0.01	0.01	0.00	0.00
Al	1.92	1.97	1.95	1.95	1.94	Al	1.94	1.95	1.95	1.96
Cr	na	0.01	0.00	0.00	0.00	Cr	na	na	na	na
Fetot	0.44	0.06	0.06	0.07		Fetot	0.42	0.46		
Fe3	0.08	0.03	0.05			Fe3	0.06	0.05	0.03	0.05
Fe2	0.39	0.43	0.44	0.53	0.50	Fe2	0.37	0.39		
Mn	0.05	0.08	0.06	0.53	0.04	Mn	0.01	0.00	0.00	0.00
Mg	0.56	0.49	0.53	0.53	0.44	Mg	0.00	0.00	0.00	0.00
Ca	0.00	0.00	0.00	0.00	0.00	Ca	0.96	0.97	0.95	0.97
Na	0.00	0.00	0.00	0.00	0.00	Na	0.00	0.00	0.00	0.00
K	0.00	0.00	0.00	0.00	0.00	K	0.00	0.00	0.00	0.00
XMg	0.59	0.53	0.55	0.50	0.47					

was analysed. It corresponds to flake-shaped phengite over-growing the main foliation.

5.2.6. Lawsonite

Lawsonite is generally present in metabasite and rarely in some carpholite-bearing samples (DU1215 and De1201c). All iron measured in lawsonite was considered as trivalent. Average composition is close to the ideal formula, e.g. $Si_{2.03}Al_{1.96}Fe^{3+}_{0.04}Ca_{1.96}O_7(OH)_2 \cdot H_2O$ for sample DU1215. The only substitution is Fe^{3+} for Al^{3+} as reported for blueschists of the Tavşanlı zone (Okay, 1980a), and for other blueschist-facies rocks of the Franciscan complex (Davis and Pabst, 1960) or the Schistes Lustrés complex (Plunder et al., 2012).

5.3. Continental rocks (Orhaneli unit)

5.3.1. Chloritoid

Chloritoid, found only in the greyschists, has X_{Mg} in the range 0.10–0.20. It shows no zoning and intra-sample variation in X_{Mg} does not exceed 0.05 (Fig. 6a; Table 3). Fe^{3+} calculated (considering $Fe^{3+} = 4 - Al$) is always <0.02 p.f.u., which indicates a low oxidation state for those rocks.

5.3.2. Phengite

White mica was observed in all greyschist samples of the Kocasu formation. It was also found in some metabasite or cherts of the Devlez formation. The Tschermak substitution between muscovite and celadonite accounts for most of the compositional variation. The Si content generally is in the range 3.3–3.6 p.f.u. whatever the considered formation (Fig. 6b). Texturally late rare phengite has lower Si contents (<3.3 p.f.u.). The pyrophyllitic contents range between 5 and 20 mol%. The mole fraction of paragonite is lower than 0.05 in the greyschist and might be up to 0.1 in some metabasite of the Devlez formation (11TAV20) in which paragonite was also measured.

5.3.3. Sodic pyroxene

Two different sodic pyroxenes were measured. In the greyschists, sodic pyroxene is very close to the jadeite end-member with $X_{jadeite}$ >0.85 (Fig. 6c), the spread being mostly due to the $Fe^{3+} = Al^{3+}$ substitution, with the core being slightly richer in Fe^{3+}, while variations in Ca/Na are small (sample OR1024; Fig. 6c). Sodic pyroxene from the metabasite of the Devlez formation displays more variation, with relatively high Fe^{3+} content and Ca/Na ratios (Fig. 6c), mostly in the aegirine-augite or aegirine fields (Fig. 6c). No systematic zoning was observed. Jadeite occurs sporadically in the cherts of the Devlez formation and has a range of Fe^{3+} contents (sample 11TAV23c, Fig. 6c). Pre-metamorphic, magmatic relict pyroxene found in some sodic amphibole–lawsonite-bearing pillow basalts and associated pillows breccias is of augitic composition (TAV1110a,b; Table 3).

5.3.4. Sodic amphibole

Sodic amphibole from the greyschists of the Kocasu formation is ferro-glaucophane to glaucophane with $X^{3+}_{Fe} < 0.10$. X_{Mg} ranges from 0.25 to 0.70, with Mg content increasing towards the rims (Fig. 6d); intra-sample variation in X_{Mg} is generally of 0.30. Sodic amphibole from the metabasite or the metachert of the Devlez formation shows variable X_{Mg} in the range 0.3–0.8 (Fig. 6d) and strong variations of Fe^{3+}, even within sample, with $0.1 < X^{3+}_{Fe} < 0.9$ (TAV1004, 11TAV20; Fig. 6d).

5.3.5. Lawsonite

Lawsonite in the Kocasu and Devlez formation in very close to the ideal formula $CaAl_2Si_2O_7(OH)_2 \cdot H_2O$, the only substitution observed being Fe^{3+} for Al^{3+} as reported for blueschists of OC2. Fe_2O_3 measured in the metabasites and in the metacherts of the Devlez formation is in

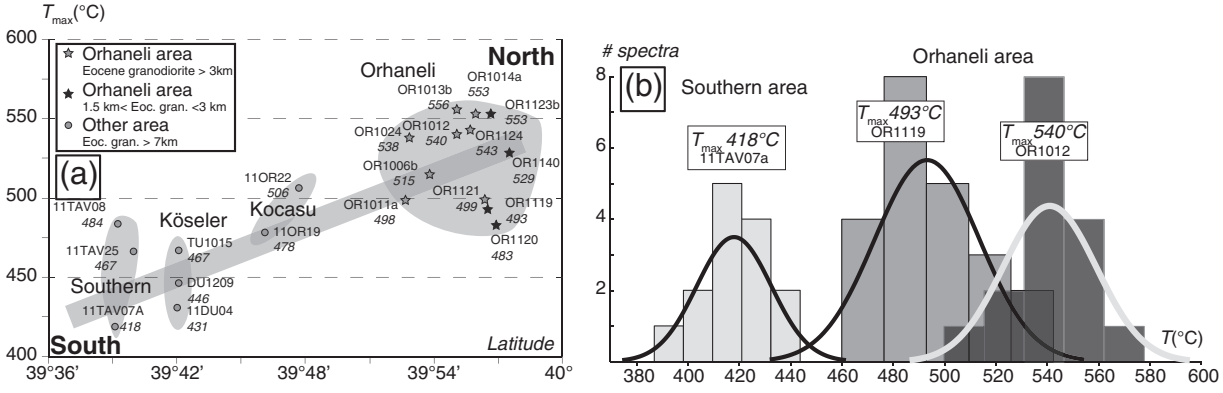

Fig. 7. Results of maximum temperature (T_{max}) obtained from Raman spectroscopy of carbonaceous material plotted against the latitude of the sample location on the geological map (Fig. 1). Distance from the main granodioritic plutons is indicated with the symbols. Temperature distribution and Gaussian fit for three selected samples.

Table 4
Maximum temperature obtained by RSCM. n, number of spectral acquisition; SD, standard deviation; SE, standard error, which is SD divided by SQRT(n).

Sample	Area		n	Av. T(°C)	SD	SE	N (°,′,″)	E (°,′,″)
OR1140	Orhaneli	Keles N	20	529	29	7	39°57′30.6″	29°14′02.8″
OR1011a		Orhan-Keles N	20	498	29	7	39°52′39.8″	29°06′24.3″
OR1012		Orhan-Keles N	16	540	16	5	39°55′05.5″	29°10′45.4″
OR1013b		Orhan-Keles N	18	556	26	6	39°55′05.5″	29°10′37.4″
OR1014a		Orhan-Keles N	19	553	30	7	39°55′59.4″	29°27′57.1″
OR1119		Orhan-Keles N	22	493	20	4	39°56′33.0″	29°02′55.6″
OR1120		Orhan-Keles N	18	483	23	5	39°56′54.7″	29°03′18.1″
OR1121		Orhan-Keles N	12	499	18	5	39°56′24.2″	29°03′56.0″
OR1123b		Orhan-Keles N	19	553	28	6	39°56′39.3″	29°05′28.5″
OR1124		Orhan-Keles N	18	543	25	6	39°55′42.2″	29°05′57.8″
OR1006b		Orhan-Keles S	19	515	31	7	39°53′48.6″	29°01′19.9″
OR1024		Orhan-Keles S	17	538	25	6	39°52′52.4″	29°05′36.5″
11TAV22	Other	Domanic	10	428	17	5	39°48′35.3″	29°34′10.3″
11TAV07a		Dursunbey	14	418	14	4	39°39′03.3″	28°24′37.6″
11TAV08		Dursunbey	18	484	33	8	39°39′14.1″	28°24′47.6″
11TAV25		Harmancik	9	467	22	7	39°39′56.6″	29°04′02.4″
11OR19		Kocasu	11	478	24	7	39°46′04.8″	28°40′55.9″
11OR22		Kocasu	14	506	27	7	39°47′43.1″	28°41′13.4″
11DU04		Koseler	13	431	22	6	39°42′02.0″	29°17′24.8″
DU1209		Koseler	20	446	20	4	39°42′04.2″	29°17′58.5″
TU1015		Koseler	20	467	27	6	39°42′03.0″	29°17′25.0″

the range 0–1.5 wt% and 1–2.2 wt% (11TAV20 and TAV1004), respectively. In the metaclastic rocks of the Kocasu formation Fe_2O_3 measured is always lower than 0.5 wt% (OR1024).

5.3.6. Garnet

Garnet observed in the metacherts of the Devlez formation is strongly zoned with spessartine-rich cores and (Fe + Ca)-richer rims (TAV1004). Typical variations are $Alm_{0.30-0.60}$-$Grs_{0.15-0.20}$-$Sps_{0.10-0.50}$-$Prp_{<0.05}$. Garnet observed in solely one metabasite sample (11TAV20) shows the following chemical variations: Alm_{60-65}-Grs_{18-20}-Sps_{5-12}-Prp_{5-15}.

6. Estimating PT conditions: Raman spectroscopy and pseudosections

6.1. Raman thermometry

The T_{max} values were calculated for 23 samples of the Orhaneli unit from the spectra as described in Beyssac et al. (2002) and part of the data come from the Plunder et al. (2013) study. The T_{max} is in the range 418–556 °C for all the samples investigated (Figs. 1c, 7a; Table 4). Spectra present a normal distribution regarding all spectra measured per sample, precluding the presence of detrital high-grade graphitic material. The typical standard deviation on T_{max} ~30 °C (Fig. 7b). No samples were collected in the contact-metamorphic aureole (~1.5 km) reported by Lisenbee (1972) and no relationship was found between the proximity of the Eocene granodiorite in the Orhaneli area (between 1.5 and 3 km and > 3 km; Fig. 1c) and the T_{max} value calculated for the greyschist samples (Fig. 7a). T_{max} shows a gradual increase from south to north. Measurement for a greenschist-facies pelitic rock of the lower part of the metamorphic sole yielded a T_{max} value of 428 °C.

6.2. PT estimates from pseudosection modelling

Two internally consistent thermodynamic datasets were used:

- for carpholite-bearing rocks the update of Berman's (1988) dataset by Pourteau et al. (2014; see their Data Repository for the thermodynamic dataset for THERIAK/DOMINO) was chosen for its incorporation of solution models developed in the last decades for pelitic high-pressure rocks. This thermodynamic database includes the solid-solution model for chlorite of Vidal and Parra (2000) and Vidal et al. (2006) with the end-members daphnite (Daph), clinochlore (Clin), Fe-amesite (Fe-Am), Mg-amesite (Mg-Am), and sudoite (Sud). For white mica, the thermodynamic model of Vidal and Parra (2000) updated with Margules parameters by Dubacq et al. (2010) was used with the following end-members: muscovite (Ms), Fe-celadonite (Fe-Cel), Mg-celadonite (Mg-Cel), pyrophyllite (Prl) and paragonite (Pg), i.e. without consideration for the low-temperature hydrated end-members. Thermodynamic data for Fe- and Mg-chloritoid and for Fe- and Mg-carpholite rely on those estimated by Pourteau et al. (2014), who refined the standard-state enthalpies of formation.
- for greyschists and metabasites, the updated database of Holland and Powell (1998) was chosen. The following solution models were used: garnet, plagioclase, chloritoid and carpholite after Holland and Powell (1998), chlorite after Holland et al. (1998), white mica after Coggon and Holland (2002), biotite after White et al. (2007), amphibole after Diener et al. (2007), clinopyroxene after Green et al. (2007). The Diener and Powell (2012) update for amphibole and clinopyroxene solution model was implemented in the tcdb55cd2.bs database of THERIAK/DOMINO for calculations considering Fe^{3+}. Bulk compositions used for pseudosection modelling are given in Table 2.

6.2.1. Metamorphic sole

One PT pseudosection was calculated for sample KO1218 collected near Çivili (Fig. 1). It was chosen due to the only slight blueschist-facies overprint. The chemical system for calculation is Na_2O–CaO–TiO_2–MnO–FeO–Fe_2O_3–MgO–Al_2O_3–SiO_2–H_2O (NaCaTMnFMASH, with F = FeO and Fe_2O_3; Table 2). Calculation was performed in the range 7–13 kbar and 600–900 °C (Fig. 8a). K_2O was neglected because it enters only in phengite composition. The Fe^{3+} amount was estimated from amphibole and pyroxene electron-microprobe analyses. Water was considered in the calculation, but its proportion was restricted to the amount present in amphibole (which makes up 50–60% of the mode).

The studied assemblage (i.e. garnet–clinopyroxene–amphibole–plagioclase–ilmenite) is stable within a large field. Using X_{Grs} isopleths, however, as well as the modal amount of clinopyroxene, PT conditions can be refined as ~11 ± 1.5 kbar and 725 ± 50 °C for the peak-temperature assemblage.

6.2.2. Ocean-derived units

Four PT pseudosections of carpholite-bearing rocks found in OC2 were calculated in the CaO–K_2O–FeO–MgO–Al_2O_3–SiO_2–H_2O

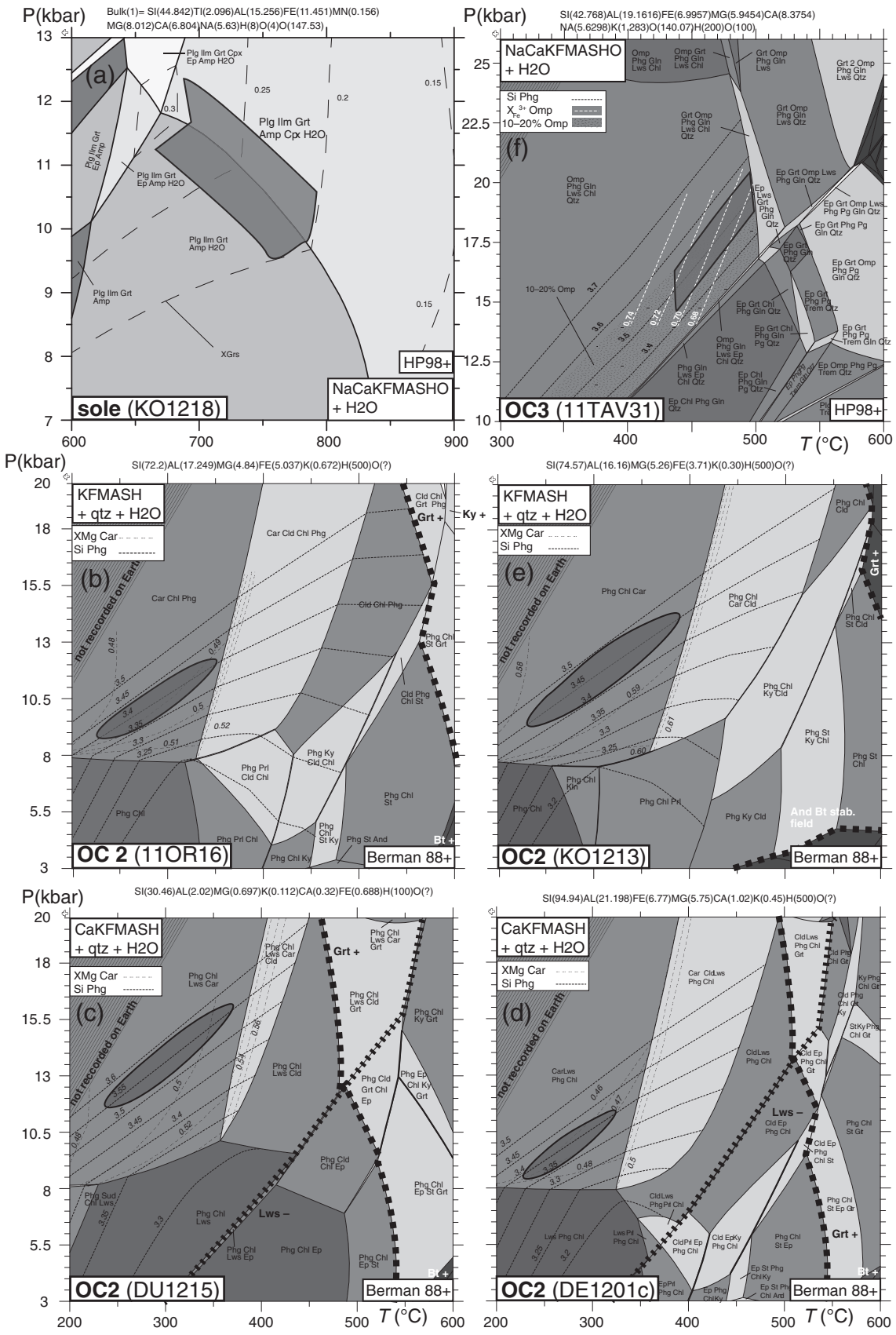

Fig. 8. PT pseudosections calculated with Theriak/Domino for samples of the metamorphic sole (a), OC2 unit (b),(c),(d) and (e) and Devlez formation (f). Bulk composition used is indicated above each grid. Chemical system and the database used are reported in the upper left part and/or the lower right part of the grid. Darker field indicate higher variance. Shape indicates the estimated PT conditions. Mineral abbreviations after Kretz (1983) except for the minerals mentioned in previous figures and Phg = phengite.

(CaKFMASH) or in the KFMASH systems. Calculations were done in the range 3–20 kbar and 200–600 °C (Fig. 8b,c,d,e). Ti was not considered in calculations, as it is present only in rutile. For bulk compositions containing Ca-bearing phases, corrections were made considering that the bulk P_2O_5 is present only in apatite (Table 2). Although Mn was measured in carpholite and some chlorite, it was not considered in the calculations, as Mn content in carpholite remains limited and no reliable thermodynamic data exist for Mn-carpholite or -chlorite in the chosen database. Moreover, Mn does not affect the composition of phengite that was used for determining the PT conditions. Ferric iron was not considered in the calculations because mineral formula recalculation indicates very low Fe^{3+} content if any. Water was considered as in excess with an activity $a(H_2O) = 1$. The topologies for the pseudosections in the KFMASH and CaKFMASH systems are alike, and are even similar to those in FMASH (Pourteau et al., 2014). The observed assemblage (carpholite–phengite–chlorite–quartz ± lawsonite) is present as a large tri-variant field spanning the conditions 200–400 °C and 7.5–20 kbar. It is limited towards high temperature by the appearance of chloritoid, which was not observed in any carpholite-bearing sample. The stability fields of kaolinite, pyrophyllite and sudoite, which have not been found during microprobe work, define the lower pressure limit. The measured Si content of phengite together with the X_{Mg} of carpholite were used together to refine the PT conditions of the studied samples. The PT conditions matching the observed mineral compositions (Fig. 5) are estimated at 10 ± 2 kbar and 300 ± 50 °C for sample 11OR16 (Fig. 8b), at 12.5 ± 2.5 kbar and 300 ± 60 °C for sample DU1215 (Fig. 8c), at 10 ± 1.5 kbar and 275 ± 50 °C for sample DE1201c (Fig. 8d) and at 11.5 ± 2.5 kbar and 300 ± 75 °C for sample KO1213 (Fig. 8e). These PT estimates can be refined by comparing the results of pseudosection modelling with the calibration of the interlayer content of white mica in carpholite-bearing rocks from the western Alps (Agard et al., 2001a). Considering 0.1–0.3 vacancy p.f.u for the investigated samples, temperature conditions can be refined to the range ~280–360 °C.

6.2.3. Units previously identified as continental-derived

The metabasite sample 11TAV31 from the Devlez formation was selected for pseudosection modelling in the NaCaKFMASHO system. Because of high Fe^{3+} content calculated in minerals (sodic amphibole and pyroxene), the last update of Diener and Powell (2012) of amphibole and clinopyroxene solid-solution model was used together with the models mentioned above for this pseudosection. The XRF bulk analysis of this sample was corrected for Ti, Ca and Si due to the presence of titanite as the only Ti-bearing phase observed (Table 2). Corrections for Ca were also made for the presence of apatite and a late carbonate vein cross-cutting the main foliation. Water was considered in excess with an activity $a(H_2O) = 1$, due to the abundance of hydrous phases and of pristine lawsonite, which imposes very CO_2-poor fluid conditions (Nitsch, 1972). The stability of the observed assemblage (sodic pyroxene–lawsonite–sodic amphibole–phengite–chlorite–quartz) is predicted over a large range of PT conditions: 300–480 °C and 10–24 kbar. Modal amounts of lawsonite/sodic pyroxene, Si content of phengite, Al^{3+}, Fe^{3+}, and X_{Mg} isopleths of sodic pyroxene were used to restrict the formation conditions to 13.5–20.0 kbar and 460 ± 30 °C (Fig. 8f).

Table 5
Predicted modal amount for modelled greyschist samples.

Sample	OR1024	OR1006b	OR1012	11OR22
Jadeite	5	7	8	4
Chloritoid	19	3	18	14
Lawsonite	4	5	0.3	
Glaucophane	12	9	10	13
Phengite	32	17	38	27
Quartz	28	59	26	41
T(°C)/P (kbar)	500 / 24.5	460 / 23.5	515 / 25	500 / 24

Four representative samples of greyschists (Kocasu formation) were selected to calculate pseudosections in the range 10–26 kbar and 300–600 °C. The system Na_2O–CaO–K_2O–FeO–MgO–Al_2O_3–SiO_2–H_2O (NaCaKFMASH) was assumed to describe the chemistry of the greyschists. Mn was neglected due to the little amount in bulk composition and the absence of Mn-bearing phases. Ti is only present in rutile and was thus not considered in calculations. Corrections were made for Ca considering that the amount of P_2O_5 measured in the bulk composition accounts only for apatite (Table 2). All pseudosections were calculated without ferric iron, as the amount of Fe^{3+} calculated in each phase is very restricted (Table 3). Given the hydrous mineral assemblages observed in thin section, water was considered in excess and its activity was set to $a(H_2O) = 1$.

The four PT pseudosections, calculated in the NCKFMASH or NKFMASH system for sample OR1012, OR1024, OR1006b (Orhaneli region) and 11OR22 (Kocasu region), have very similar topologies. The assumed peak-pressure assemblage glaucophane–jadeite–chloritoid–phengite–quartz ± lawsonite is reproduced as a triangular-shaped field in each case. The maximum spread of this field is from 400 to 500 °C and between 20 to 26 kbar. It is limited by the presence of carpholite towards the low temperatures and by the appearance of garnet at higher temperatures. None of these minerals has been observed in any of the relevant rocks. The lower pressure boundary is made by the appearance (up pressure) of clinopyroxene with $X_{Jadeite} > 0.9$ at ~20 kbar or by the disappearance of paragonite. The high-pressure boundary is marked by the appearance of a carpholite + garnet field, an uncommon assemblage in Mn-poor systems, only reported from the North Qilian suture zone, NW China (Song et al., 2007). The Si content of phengite was used together with the X_{Mg} of chloritoid and the $X_{Jadeite}$ to deduce the PT conditions matching the observed paragenesis. These are estimated at 25 ± 1 kbar and 515 ± 20 °C for sample OR1012, at 24.5 ± 1 kbar and 500 ± 25 °C for sample OR1024, at 24 ± 1 kbar and 500 ± 25 °C for sample 11OR22 and at 23.5 ± 1.5 kbar and 460 ± 30 °C for sample OR1006b. Modal abundances for peak PT assemblages are given in Table 5 and are consistent with observations at thin-section scale except for sample 11OR22 where glaucophane is predicted to account for >10% of the mode and is only observed as tiny relictual mineral (<5%). Constraints on decompression paths are set by the appearance of garnet at 450–550° for pressure between 10 and 20 kbar depending on the bulk composition, by the fact that neither the breakdown of lawsonite to epidote below 15 kbar nor the appearance of biotite are observed, and by the coincidence of T_{max} and the estimated temperature for peak pressure (Fig. 8).

7. Discussion and interpretation

7.1. - PT conditions for the different units of the Tavşanlı zone

The PT conditions derived for the Tavşanlı rocks are summarized in Fig. 10a and critically discussed below, from top to bottom.

(1) PT estimates for the top part of the HT metamorphic sole (11 ± 1.5 kbar and 725 ± 50 °C) are higher than those previously reported for similar samples (Okay et al., 1998; Fig. 10a) due to the incorporation of previously not recognized pyroxene. Such PT conditions are consistent with those of metamorphic soles found immediately beneath the Semail (Oman; Gnos, 1998) or Vourinos ophiolites (Myhill, 2011). Thanks to recent improvements in solution models for clinopyroxene (Diener and Powell, 2012), our estimates are probably more robust than previous, comparable studies. Uncertainties come from (1) the bulk-rock composition used for the pseudosection calculation, which may be affected by minor compositional changes related to the high-pressure overprint (i.e., addition of water and redox changes; Fig. 4a) and (2) the initial HT plagioclase composition, which had to be estimated from the relative modal amounts of lawsonite and albite replacing plagioclase.

(2) Carpholite-bearing rocks of the OC2 accretionary complex yielded PT conditions of 11.5 ± 3.5 kbar and 350 ± 50 °C on average, which supports the preliminary result of Plunder et al. (2013). These PT estimates confirm the large metamorphic gap between OC1 and OC2, which was already apparent in terms of lithology (see Geological setting). As the OC2 samples come from areas far apart (i.e., >50 km along strike), the OC2 unit either corresponds to distinct pieces of various units detached at a common decoupling depth, or to thin slivers of a larger, tectonically stripped oceanic unit. The timing of its/their detachment from the sinking slab remains poorly constrained (i.e. between 95 and 80 Ma).

(3) For the Devlez formation, PT estimates (13.5–20 kbar and 440–500 °C) lie close to the lawsonite–epidote transition (Fig. 8f). They are supported by the occurrence of epidote in some samples coexisting with lawsonite or included in lawsonite, in sodic amphibole or in garnet (11TAV20). These PT conditions are somewhat more loosely constrained than those of the Kocasu formation, yet distinguishable (Fig. 10a; see below). The exercise of pseudosection modelling of the Devlez formation also shows how very common rocks (glaucophane + lawsonite ± sodic pyroxene) remain difficult to model. The well-known, ubiquitous glaucophane–lawsonite assemblage (Alps, Corsica, Tavşanlı, Franciscan) is difficult to reproduce in pseudosections and is even not present in some reference calculations that predict a very wide stability field for sodic pyroxene or calcic amphibole towards low temperature (Diener and Powell, 2012). This may simply reflect the still imperfect solid-solution modelling and even end-member thermodynamic data for some of the key phases, blue amphibole in particular.

(4) Pseudosection modelling of the continental Kocasu formation suggests equilibration at 470–510 °C and 23–25 kbar for the typical jadeite–glaucophane–chloritoid–phengite–quartz ± lawsonite assemblage found in the north of the study area. Thermobarometric results are supported by the independent RSCM T_{max} results ranging between 480-550 °C for the same area (Figs. 1c,7). These T_{max} values for the Orhaneli unit and those reported in Plunder et al. (2013) are systematically higher than previous maximum T estimates (430 ± 30 °C; Okay and Kelley, 1994; Okay, 2002), which implies a slightly warmer metamorphic gradient than previously thought (i.e., ~7 °C/km vs. 4-5 °C/km; Okay, 2002).

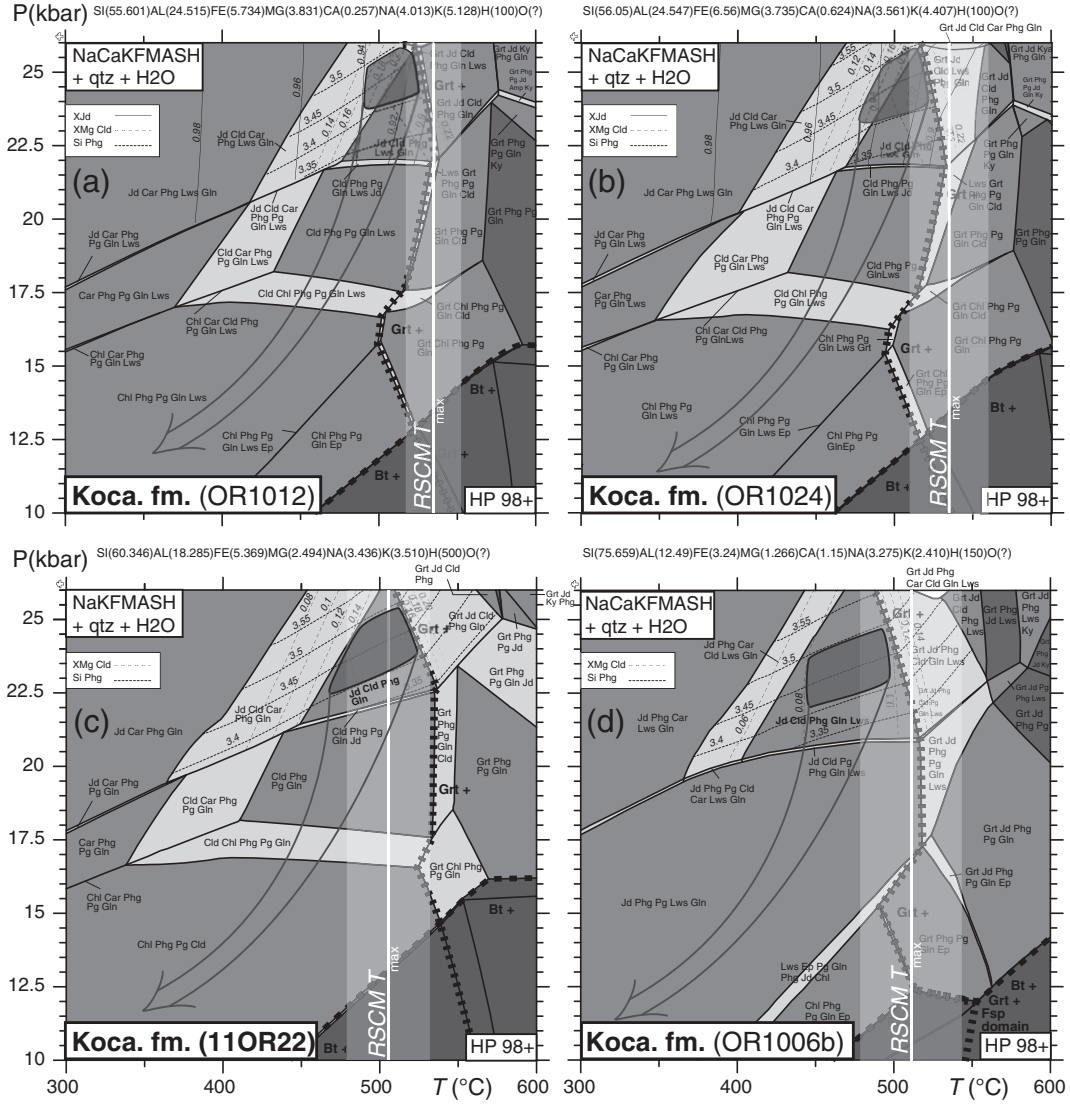

Fig. 9. PT pseudosections calculated with Theriak/Domino for samples of the Kocasu formation. Shape indicates the estimated PT condition. Maximum temperature from Raman spectroscopy on carbonaceous material is indicated to show the good agreement between two independent methods. Indicative retrograde path is constrained on the basis of the observed assemblage, the stability of lawsonite in studied samples and the absence of regional heating after the HP metamorphic event. See text for discussion. Mineral abbreviations after Kretz (1983) except for the minerals mentioned in previous figures and Fsp = K-feldspar.

Those estimates are consistent with the Grt–Na Cpx–Lws–Gln paragenesis found in a metabasite of the Orhaneli region (OR1111, metabasite slice atop the Kapanca metagranitoid; Okay et al., 2008). The predicted appearance of garnet for this rock-type lies between 500 and 550 °C at 20 kbar (Fig. 8f; Diener and Powell, 2012).

For the continental samples OR1210 and OR1024, the predicted mineral stability fields include carpholite (Fig. 9a), which is not observed in these samples. This probably stems from inaccurate thermodynamic data for Fe-carpholite (see Pourteau et al., 2014). Uncertainties on isopleths, such as the Si content of phengite, X_{Mg} of chloritoid, jadeite content of pyroxene, are difficult to assess but likely within the range of uncertainties of the database (i.e. ±50 °C and ± 1.5 kbar).

The RSCM results also reveal a north-to-south decrease in T_{max} (Fig. 7a), which is consistent with the absence of the jadeite–glaucophane–chloritoid–phengite–quartz ± lawsonite assemblage in the south, where chloritoid–glaucophane or jadeite occur instead. The lack of east-west structural discontinuities or deformation trends (Plunder et al., 2013) suggests that this temperature decrease may be gradual and implies (assuming a similar PT gradient) a lesser burial in the south of maximum 20 km (i.e ~6-7 kbar). This is consistent with a structural thickness of at most 1 km for the Kocasu formation and the less intense penetrative deformation observed in the southern part (Supplementary material). Noteworthily, the lack of any relationship between the T_{max} measured in the Kocasu samples and the Eocene granodioritic intrusions (Fig. 7a) demonstrate that these intrusions did not disturb the earlier, HP metamorphic thermal patterns.

Contrasting PT estimates are found for the chert-rich Devlez formation and the Kocasu formation, once thought to belong to a single Orhaneli unit (Okay, 1986). By contrast to the regional-scale distribution of the Kocasu and İnönü formations, which extend from Dursunbey to Sivrihisar (~300 km from west to east), the Devlez formation is only found in our study area. Deformation patterns for the Devlez formation also differ significantly from those found in the rest of the Orhaneli unit, locally and across the whole region (Davis and Whitney, 2006; Davis, 2011; Monod et al., 1991; Plunder et al., 2013; e.g., stretching lineations, in particular, systematically strike ~ N160 instead of ~ N020; see Supplementary material). In addition, the İnönü marble commonly grades from thick-bedded carbonates to lithologies quite distinct (i.e., impure marly marbles) from the ones in Devlez (alternating metagreywackes and metabasites; Servais, 1981). The Devlez formation is therefore regarded as originating from near the northern edge of the passive continental margin of the Anatolide-Tauride Block yet has an oceanic affinity, and is consequently referred to as OC3 below. This interpretation is supported by the existence of a tectonic contact between the İnönü formation and the Devlez formation near the locality of Dombayçayırı, marked by a 5–10 metre thick crushed calcschist layer. The continental Orhaneli unit would thus be restricted to the Kocasu and the İnönü formations (see cross section on Fig. 1).

Fig. 10b shows how these new PT estimates refine previous ones for the Tavşanlı units (Fig. 10a,b).

7.2. From subduction inception to continental subduction: accretion, underplating and exhumation during progressive cooling

The stacking of the Tavşanlı units provides some indications on their relative timing of accretion, underplating and exhumation (Fig. 11), despite the lack of radiometric data, which are only available for OC3 (*ca.* 80 Ma, Rb/Sr ages; Sherlock et al., 1999) and for the Afyon Zone to the south (70–65 Ma, Ar/Ar ages; Pourteau et al., 2013). Essential field relationships and structural details are outlined below for the various units (more details can be found in Plunder et al., 2013).

OC1 correspond to a coherent 100–1000 m thick oceanic unit, with imbricate slices that may be traced for 500 m to a few kilometres, of weakly deformed but incipiently metamorphosed basalts and radiolarian cherts. OC2 is much more strained and probably represents an extremely thinned (<100 m) oceanic unit, extending across a few hundred metres and only observed in some localities (Fig. 1a). OC3 is a ~1 km thick and coherent oceanic unit intimately linked to the continental Orhaneli unit. The contact between OC1 and OC2 is marked by a sharp change in metamorphic grade (from virtually unmetamorphosed to blueschist grade rocks) and a few metres thick serpentinite layer (in Ketenlik or Dutluca regions). In all places, the contact between the metamorphic sole and OC1 is marked by a sharp contrast in metamorphic grade and in lithologies (e.g., at Çivili, south of Tavşanlı and in the Küthaya region).

(1) Tectonic contacts in the study area always yield a consistent stacking pattern with, from top to bottom, (i) the ophiolite, (ii) the metamorphic soles partially reequilibrated under HP conditions, (iii) voluminous and continous imbricates slices of OC1 (>80% of the mapped OC) with incipient BS conditions, (iv) thin, strongly deformed OC2, (v)restricted exposures of OC3 and (vi) finally the Orhaneli unit, to which OC3 is intimately

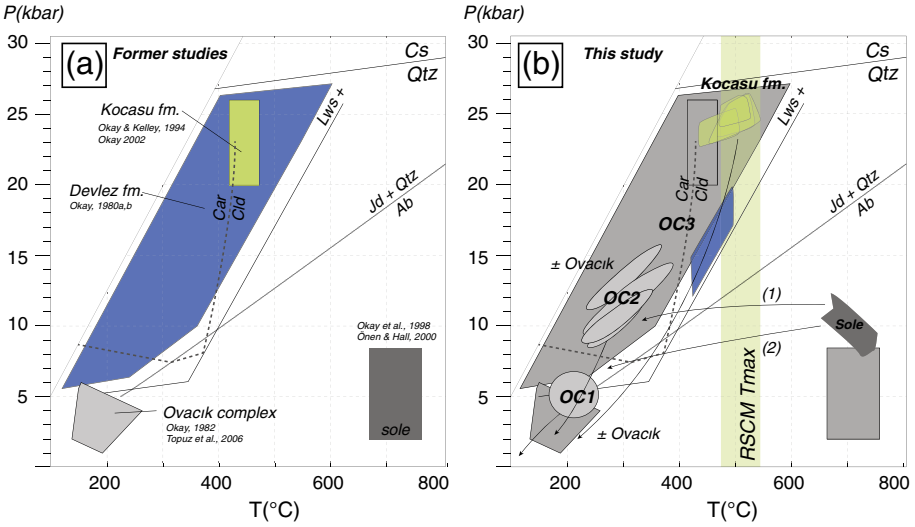

Fig. 10. (a) PT conditions estimates for the Tavşanlı zone prior to this study; (b) Revised PT conditions from this study.

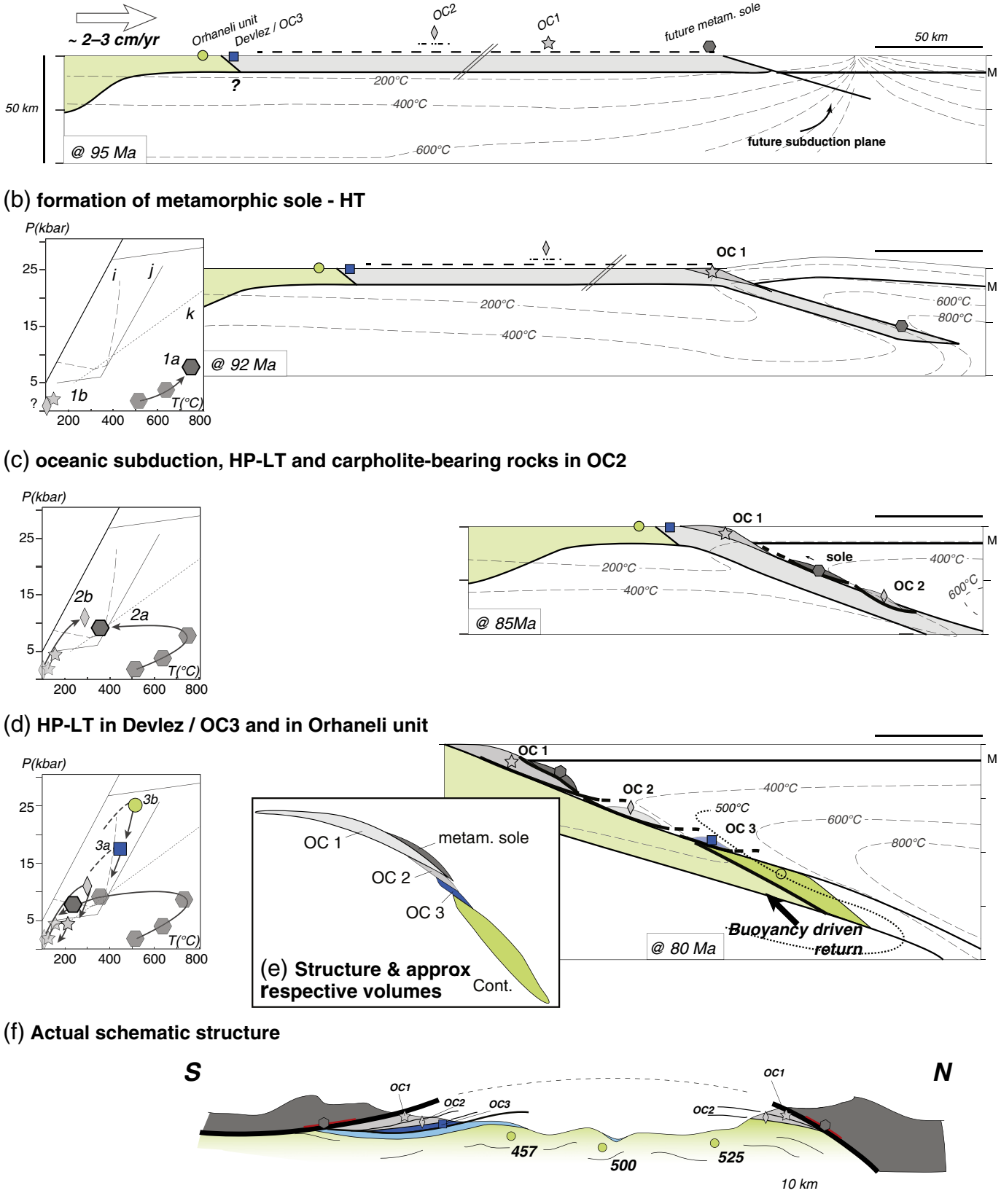

Fig. 11. Schematic evolution of the Neotethyan ocean since the initiation of an intra-oceanic subduction, the oceanic and continental subduction. See text for detail. i, j and k correspond to reaction labelled on Fig. 10.

linked). The downward pressure increase of the nappe stack and the pressure gaps point to the existence of net extensional offsets between the various units (i.e., OC1/OC1 and OC2/OC3). Structural relationships (i.e., OC3 sandwiched between OC2 and the Orhaneli unit) and paleogeographic constraints (OC2 being clearly oceanic and OC3 transitional to the continent) suggest that OC2 was likely underplated before OC3, and OC3 before the continental Orhaneli unit. The buoyancy-driven exhumation of the large, coherent Orhaneli continental unit (such as in the Western Alps; Angiboust et al., 2009; Plunder et al., 2012) may have contributed to scrapping off OC3 and/or OC2 on its way up the plate interface. Radiometric constraints are needed to unravel whether OC2 was already exhumed before OC3 reached its maximum burial depth, or whether both units were exhumed coevally with the continental margin. We speculate that the large volumes of OC1 probably correspond to a longer-lived accretion and underplating history. In any case, given its structural position beneath OC1, OC2 cannot have been exhumed to depths of OC1 before OC1 was accreted.

(2) The HP-LT overprint of the metamorphic sole records the cooling of the subduction zone through time from ca. 700 to 300 °C (Fig. 10b). Whether the sole cooled at constant depth (arrow 1; Fig. 10b) or during its exhumation (arrow 2) is unclear. This blueschist overprint of the sole requires a cooler, more mature thermal regime of the subduction zone, which implies that the metamorphic sole cannot have been significantly exhumed during the earliest and warm stages of subduction (i.e., around 93–90 Ma). The underplating of significantly colder oceanic HP units likely contributed to this cooling. The structural position of the sole on top of both OC1 and OC2, and the higher P conditions witnessed by the sole with respect to OC1, require that the metamorphic sole was emplaced on OC1 as a thrust (and exhumed with respect to the mantle part of the ophiolite since its maximum burial depth exceeds the ophiolite thickness, as for most metamorphic soles worldwide; Wakabayashi and Dilek, 2003) and was exhumed prior to and independently of OC2 (Wakabayashi and Dilek, 2003).

Using the above structural and time constraints and available palaeogeographic data for the Neotethys, we herein show that the HP-LT Tavşanlı units fit on a simple convergence history (Fig. 11).

Kinematic and palaeogeographic reconstructions (MEBE maps: Barrier and Vrielynck, 2008; van Hinsbergen et al., 2010) suggest that the Neotethyan ocean at 95 Ma extends across ~ 700-800 km from N to S. From this stage to Paleocene closure of the Neotethys, this estimate yields an average convergence velocity of 2–3 cm/yr between the Anatolide-Tauride block and Eurasia. Considering that (1) intra-oceanic subduction started at ~95-92 Ma (see Çelik et al., 2011, for a compilation; Önen, 2003) and that (2) HP-LT metamorphism in OC3, outboard of the continental margin, occurred at ~80 Ma (Sherlock et al., 1999), subduction initiation must have occurred ~300 km north of the Anatolide-Tauride block. Noteworthily, the depths reached by OC2-3 cannot be explained if subduction initiated too close to the Anatolide-Tauride margin. Intra-oceanic subduction probably initiated at some inherited discontinuity (Fig. 11a; Gurnis et al., 2004; Hacker, 1990, 1991; Nicolas and Le Pichon, 1980), at a ridge or in its vicinity. Indeed, the nature and age of the obducted ophiolite and the temperature reached by the metamorphic sole both require the existence of a young, buoyant oceanic lithosphere in the southern Neotethys, possibly as a propagating basin (see Rioux et al., 2013 and references therein) formed in the earlier rifted Neotethyan realm (i.e., during the Triassic as shown by radiolarite ages in OC1 and alkaline magmatism documented in the Menderes Massif and Afyon Zone; Akal et al., 2011). The ridge in Fig. 11a thus represents a proxy for such a young, buoyant oceanic lithosphere. This sketch also implicitly assumes the existence of one single ophiolite sheet extending ~400 km across, from Tavşanlı in the north to the Lycian nappes in the south (removing the late extension in the Menderes consistently yields a minimum southward overthrust of 300 km). The thermal structure of Fig. 11 is derived from recent thermomechanical modelling performed with similar parameters for the Oman obduction (i.e. 400 km of convergence over 10 My and inversion at the ridge; Duretz et al., submitted for publication; see also earlier thermo-kinematic models by Hacker, 1990, 1991).

Fig. 11 shows a possible evolution matching equilibrium depths and PT paths, the relative position of the units and the relative chronology of exhumation.

Shortly after the initiation, at ~93–92 Ma, rocks of the downgoing plate must have reached depths of ~30 km, as shown by the PT estimates for the metamorphic sole (11 kbar – 725 °C). The thermal regime of the subduction zone is still warm, with a geotherm of ~20–25 °C/km but isotherms have started to be deflected downward, as observed in present subduction zones (Peacock, 1993, 1996; Van Keken et al., 2011). Accretion might have already started at shallow levels with rocks of OC1 unit being scraped-off at the backstop.

At ~85 Ma, the thermal regime of oceanic subduction has cooled to ~10–12 °C/km, as shown by PT estimates for OC2. The OC2 slices are detached from the sinking slab at depths of ~30-40 km, possibly as a result of changes in mechanical coupling along the subduction interface (see § 7.3). The metamorphic sole has probably cooled between its formation (at ~93–92 Ma) and 85 Ma as suggested by blueschist-facies overprint. Cooling of the metamorphic sole, in any case, has to take place before peak burial of OC2, since the metamorphic sole is never found atop OC2.

Around ~80 Ma, OC3 (i.e., Devlez unit) reaches its peak-pressure conditions at 13.5–19 kbar / 425–480 °C and is detached from the slab. Exhumation of OC2 is suggested to initiate around this time for consistency between estimated PT conditions and the thermal evolution of the subduction zone. The Orhaneli unit reaches 23–25 kbar / 470–510 °C within a short time span (a few My?). The exhumation of the coherent, relatively undeformed continental Orhaneli unit (Plunder et al., 2013) might have been favoured by its net buoyancy (Brun and Faccenna, 2008; Chemenda et al., 1995) and/or by changes in the mechanical coupling along the subduction interface at depths of 70–80 km. This ascent of the continental units likely contributed to the exhumation of the previously detached OC2 and OC3.

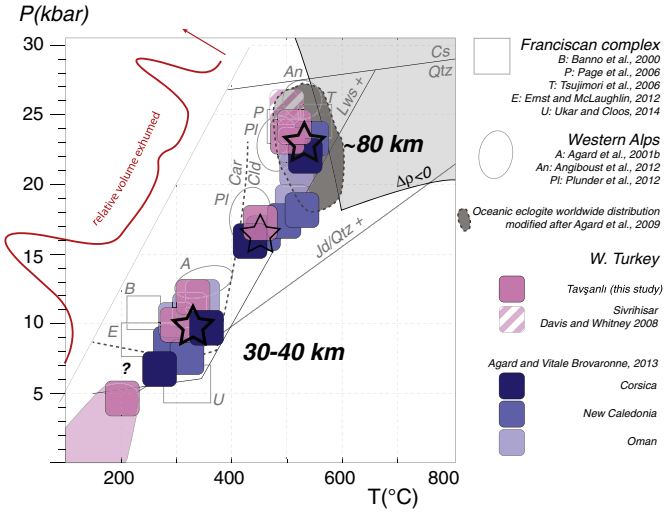

Fig. 12. Plot of maximum PT conditions for each defined tectonic unit in W. Turkey, Oman, New Caledonia, Corsica, the Schistes Lustrés and the Franciscan complex. Grey field: domain of negative buoyancy for the oceanic crust compared to the adjacent mantle after Agard et al. (2009). The red curve indicates qualitatively the volume exhumed from the involved depths.

This first-order tectonic reconstruction suggests that the Tavşanlı zone corresponds to a reworked yet single subduction interface with rock units documenting accretion, underplating and exhumation dynamics along a plate interface. The positions of OC1-2-3 in this reconstruction are not unique, however, and absolute age data are needed to better constrain timescales and processes.

7.3. Exhumation dynamics and mechanical coupling along the subduction interface

Unlike the Oman case study (for a comparison, see Plunder et al., 2013), several metamorphosed HP oceanic slices units are sandwiched between the ophiolite (and its metamorphic sole) and the Orhaneli continental unit. Three groups of PT conditions have been identified for these HP complexes: (1) <8 kbar and <250 °C for the poorly metamorphosed yet lawsonite-bearing OC1 unit; (2) 11.5 ± 3.5 kbar and 350 ± 50 °C for the low-grade HP carpholite-bearing OC2; (3) 17 ± 3 kbar and 450 ± 50 °C for the HP glaucophane–lawsonite-bearing OC3 .

These slices of upper oceanic crust (i.e., basalt + variable amounts of pelagic sediments) were detached from the slab at distinct depths and in very contrasting volumes too (Fig. 11e): the limited exposures of OC2 (less than 200 km^2 over a 12 500 km^2 area) or OC3 constrast with the voluminous and extensive OC1. The OC2 and OC3 units may have been thinned and/or stripped on exhumation but are indeed by far (<10%) less abundant than OC1. The OC1 unit probably represents a metamorphosed equivalent of the offscrapped oceanic upper-crustal material of the Hawasina units in Oman.

Exhumation of oceanic rocks is a fundamentally discontinuous process acting over short-lived time periods in the lifetime of a subduction zone (i.e., ~10 My; Agard et al., 2009). The Tavşanlı units can thus potentially provide clues on the following open questions:

(i) do exhumed rocks primarily originate from specific depths, thereby pointing to specific conditions of mechanical coupling, or from all along the subduction interface?
(ii) is it the exhumation and/or the detachment that is a discontinuous process (or both)?

Fig. 12 suggests that specific depths may be the answer to the first question. Fig. 12 indeed shows that PT conditions for OC2, OC3 and continental Kocasu units match those proposed for the Franciscan complex, the W. Alps (Schistes Lustrés complex) or for Oman, Corsica and New Caledonia, all of which represent well-documented examples of accretionary processes in subduction zones without or prior to collision (Agard and Vitale-Brovarone, 2013; Agard et al., 2001b; Angiboust et al., 2012; Banno et al., 2000; Ernst and McLaughlin, 2012; Page et al., 2006; Plunder et al., 2012; Tsujimori et al., 2006; Ukar and Cloos, 2014; Wakabayashi, 2013). It therefore seems that the initial setting (and the age of subduction) does not much affect the detachment and or exhumation depths, a least for cold or mature (cooled) subduction zones.

The two better constrained, major depth clusters, at ~30–40 km and ~80 km, are probably not fortuitous, as they correspond to boundaries where a major change in mechanical coupling is documented or expected (Fig. 12). The PT estimates for the eclogite-facies units of Oman, Corsica, New Caledonia, California, W. Alps and Turkey are similar to the low-temperature worldwide oceanic eclogite distribution (Fig. 12; Agard et al., 2009). Mechanical coupling indeed decreases down-dip of the seismogenic zone (~30-40 km; Yoshioka et al., 2004) and likely resumes at ~80 km (Syracuse et al., 2010; Wada and Wang, 2009), a depth below which the densification of oceanic rocks will further prevent their return, unless exhumation is assisted by buoyancy-driven exhumation of continental material (Agard et al., 2009, 2010).

The detachment of units such as OC2 is consistent with previous reports of regional-scale exhumation from similar depths (Monié and Agard, 2009) and with the depths of detachment hypothesized by Singh et al. (2008) on the base of seismic evidence. These particular depths coincide with the down-dip end of the seismogenic zone, the location of episodic tremor and slip in present-day subduction zones (Rogers and Dragert, 2003) and some serpentinite dehydration reactions occurring in the sinking slab (Schwartz et al., 2013). It is therefore possible that dehydration reactions may help localize deformation and the detachment of 100 m-500 m thick units from the downgoing plate oceanic upper crust (i.e., sediments and a few basalts), preluding to later exhumation.

The OC1 unit, on the other hand, might correspond to a shallow accretionary wedge with km-scale units underplated to depths of 15-20 km as imaged by Calvert (2004) beneath northern Cascadia.

The fact that fewer PT estimates lie in between the two depth clusters (Fig. 12) suggests that, although detachment is likely chiefly depth-dependent, the depths of mechanical coupling changes may vary as a function of subduction zone parameters and this should be further explored.

The results presented here also provide no clue, unfortunately, to answer the second question. We tentatively suggest that, if the detachment is a depth-dependent process controlled by interplate mechanical coupling, then one should expect later exhumation to be rather controlled by large-scale, lithospheric-scale boundary conditions (such as slab-rollback and/or kinematic reorientations; Baldwin et al., 2004; Brun and Faccenna, 2008). In our view, mechanical coupling would control the spatial discontinuity of exhumation while geodynamic boundary conditions would control exhumation discontinuity through time (i.e., the possibility of effective exhumation).

8. Conclusions

The Tavşanlı metamorphic units provide a unique record, over a relatively short time span (i.e., <15 My), of a progressively cooling subduction zone, from subduction inception within the Neotethys to continental subduction (from ~25–30 °C/km to ~7 °C/km):

(1) The new PT conditions and observations presented here indicate that the HP-LT nappe stack of the Tavşanlı zone comprises, from top to bottom, five distinct tectonic units: the ophiolite and its metamorphic sole (11 kbar and 750 °C, with PT conditions decreasing downward), oceanic complexes OC1 (4-8 kbar and 250-300 °C), OC2 (11 kbar and 350 °C) and OC3/Devlez (17 kbar and 450 °C), and the continental Orhaneli unit (24 kbar and 500 °C).
(2) PT estimates, field observations and insights from thermomechanical numerical modelling show that the Tavşanlı units fit in a simple geodynamic scenario and that they provide constraints on the relative slicing, stacking (shallow accretion for OC1; underplating with high internal strain for OC2, or only low strain for OC3 and Orhaneli) and exhumation of tectonic units along various depths of a single subduction interface.

We herein show that PT estimates for the Tavşanlı zone overlap with those proposed for similar settings (i.e., oceanic subduction followed or not by continental subduction but not by thorough collision: New Caledonia, Oman, Franciscan complex, Corsica, W. Alps), in particular at 300 °C–12 kbar and 500 °C–23 kbar (and to a lesser extent at 450 °C–17 kbar), and point to depth clusters of 30-40 and 70-80 km.

We therefore propose that the slicing of km-scale units occurs in subduction zones at specific depths where major coupling changes occur along the plate interface: at 30-40 km (downdip of the seismogenic zone) and 70-80 km (where mechanical coupling between the two plates resumes and where eclogites contribute critically to densification; Agard et al., 2009; Syracuse et al., 2010; Wada and Wang, 2009). We finally speculate that detachment is a depth-dependent process controlled by interplate coupling whereas later exhumation is rather

controlled by large-scale, lithospheric-scale boundary conditions (such as slab-rollback and/or changes in kinematics).

Supplementary data to this article can be found online at http://dx.doi.org/10.1016/j.lithos.2015.01.007.

Acknowledgements

The authors are indebted to the PHC Bosphorus joint project (26289UD and TUBITAK 111Y137). Part of the work was funded by the ANR project O:NLAP granted to Ph. A. and through IUF. Detailed review by M. Bröcker and J. Wakabayashi were much appreciated and helped improve the manuscript. Guest editor D. Castelli is thanked for accepting this contribution to the IEC volume. H. Whitechurch is warmly thanked for providing the whole-rock analysis and for discussions about Anatolian ophiolites. D. J. J. van Hinsbergen is thanked for helping us to improve a previous version of the manuscript. Al. P. thanks B. Dubacq for numerous discussions about PT estimates during the preparation of this work. D. Deldicque is thanked for Raman and SEM access at ENS. The CAMPARIS analytical platform is thanked for access to EPMA facilities and assistance at Univ. Paris 6.

References

Abers, G.A., van Keken, P.E., Kneller, E.A., Ferris, A., Stachnik, J.C., 2006. The thermal structure of subduction zones constrained by seismic imaging: Implications for slab dehydration and wedge flow. Earth and Planetary Science Letters 241, 387–397.

Agard, P., Vitale-Brovarone, A., 2013. Thermal regime of continental subduction: The record from exhumed HP-LT terranes (New Caledonia, Oman, Corsica). Tectonophysics 601, 206–215.

Agard, P., Vidal, O., Goffe, B., 2001a. Interlayer and Si content of phengite in HP-LT carpholite-bearing metapelites. Journal of Metamorphic Geology 19, 479–495.

Agard, P., Jolivet, L., Goffé, B., 2001b. Tectonometamorphic evolution of the Schistes Lustrés complex: implications for the exhumation of HP and UHP rocks in the western Alps. Bulletin de la Societe Geologique de France 172, 617–636.

Agard, P., Yamato, P., Jolivet, L., Burov, E., 2009. Exhumation of oceanic blueschists and eclogites in subduction zones: Timing and mechanisms. Earth-Science Reviews 92, 53–79.

Agard, P., Searle, M.P., Alsop, G.I., Dubacq, B., 2010. Crustal stacking and expulsion tectonics during continental subduction: P-T deformation constraints from Oman. Tectonics 29, TC5018.

Akal, C., Koralay, O.E., Candan, O., Oberhänsli, R., Chen, F., 2011. Geodynamic Significance of the Early Triassic Karaburun Granitoid (Western Turkey) for the Opening History of Neo-Tethys. Turkish Journal of Earth Sciences 20, 255–271.

Altiner, D., Koçyigit, A., Farinacci, A., Nicosia, U., Contin, A., 1991. Jurassic-lower Cretaceous stratigraphy and paleogeographic evolution of the southern part of North-Western Anatolia (Turkey). Geologica Romana 28, 13–80.

Angiboust, S., Agard, P., Jolivet, L., Beyssac, O., 2009. The Zermatt-Saas ophiolite: the largest (60-km wide) and deepest (c. 70-80 km) continuous slice of oceanic lithosphere detached from a subduction zone? Terra Nova 21, 171–180.

Angiboust, S., Langdon, R., Agard, P., Waters, D., Chopin, C., 2012. Eclogitization of the Monviso ophiolite (W. Alps) and implications on subduction dynamics. Journal of Metamorphic Geology 30, 37–61.

Baldwin, S.L., Monteleone, B.D., Webb, L.E., Fitzgerald, P.G., Grove, M., Hill, E.J., 2004. Pliocene eclogite exhumation at plate tectonic rates in eastern Papua New Guinea. Nature 431, 263–267.

Banno, S., Shibakusa, H., Enami, M., Wang, C.-L., Ernst, W.G., 2000. Chemical fine structure of Franciscan jadeitic pyroxene from Ward Creek, Cazadero area, California. American Mineralogist 85, 1795–1798.

Barrier, E., Vrielynck, B., 2008. MEBE: Palaeotectonic maps of the middle east. Tectono — sedimentary — palinspastic maps from Late Norian to Pliocene. CGMW/CCGM, Paris (14 maps).

Berman, R.G., 1988. Internally-consistent thermodynamic data for minerals in the system Na_2O-K_2O-CaO-MgO-FeO-Fe_2O_3-Al_2O_3-SiO_2-TiO_2-H_2O-CO_2. Journal of Petrology 29, 445–522.

Beyssac, O., Goffe, B., Chopin, C., Rouzaud, J.-N., 2002. Raman spectra of carbonaceous material in metasediments: a new geothermometer. Journal of Metamorphic Geology 20, 859–871.

Beyssac, O., Goffé, B., Petitet, J.-P., Froigneux, E., Moreau, M., Rouzaud, J.-N., 2003. On the characterization of disordered and heterogeneous carbonaceous materials by Raman spectroscopy. Spectrochimica Acta Part A: Molecular and Biomolecular Spectroscopy 59, 2267–2276.

Bragin, N.Y.U., Tekin, U.K., 1996. Age of radiolarian-chert blocks from the Senonian Ophiolitic Melange (Ankara, Turkey). The Island Arc 5, 114–122.

Brun, J.-P., Faccenna, C., 2008. Exhumation of high-pressure rocks driven by slab rollback. Earth and Planetary Science Letters 272, 1–7.

Calvert, A.J., 2004. Seismic reflection imaging of two megathrust shear zones in the northern Cascadia subduction zone. Nature 428, 163–167.

Candan, O., Çetinkaplan, M., Oberhänsli, R., Rimmelé, G., Akal, C., 2005. Alpine high-P/low-T metamorphism of the Afyon Zone and implications for the metamorphic evolution of Western Anatolia, Turkey. Lithos 84, 102–124.

Çelik, Ö.F., Marzoli, A., Marschik, R., Chiaradia, M., Neubauer, F., Öz, I., 2011. Early–Middle Jurassic intra-oceanic subduction in the İzmir-Ankara-Erzincan Ocean, Northern Turkey. Tectonophysics 509, 120–134.

Chemenda, A.I., Mattauer, M., Malavieille, J., Bokun, A.N., 1995. A mechanism for syn-collisional deep rock exhumation and associated normal fault: results from physical modeling. Earth and Planetary Science Letters 132, 225–232.

Coggon, R., Holland, T.J.B., 2002. Mixing properties of phengitic micas and revised garnet-phengite thermobarometers. Journal of Metamorphic Geology 20, 683–696.

Davis, P.B., 2011. Petrotectonics of lawsonite eclogite exhumation: Insights from the Sivrihisar massif, Turkey. Tectonics 30, TC1006.

Davis, G.A., Pabst, A., 1960. Lawsonite and pumpellyite in glaucophane schist, north berkeley hills, California. American Journal of Science 258, 689–704.

Davis, P.B., Whitney, D.L., 2006. Petrogenesis of lawsonite and epidote eclogite and blueschist, Sivrihisar Massif, Turkey. Journal of Metamorphic Geology 24, 823–849.

de Capitani, C., Brown, T.H., 1987. The computation of chemical equilibrium in complex systems containing non-ideal solutions. Geochimica et Cosmochimica Acta 51, 2639–2652.

de Capitani, C., Petrakakis, K., 2010. The computation of equilibrium assemblage diagrams with Theriak/Domino software. American Mineralogist 95, 1006–1016.

Dercourt, J., Ricou, L.E., Vrielynck, B., 1993. Tethys Palaeoenvironmental maps Atlas and Explanatory Notes.

Diener, J.F.A., Powell, R., 2012. Revised activity-composition models for clinopyroxene and amphibole. Journal of Metamorphic Geology 30, 131–142.

Diener, J.F.A., Powell, R., White, R.W., Holland, T.J.B., 2007. A new thermodynamic model for clino- and orthoamphiboles in the system Na_2O-CaO-FeO-MgO-Al_2O_3-SiO_2-H_2O-O. Journal of Metamorphic Geology 25, 631–656.

Dilek, Y., Whitney, D.L., 1997. Counterclockwise P-T-t trajectory from the metamorphic sole of a Neo-Tethyan ophiolite (Turkey). Tectonophysics 280, 295–310.

Droop, G.T.R., 1987. A general equation for estimating Fe^{3+} concentrations in ferromagnesian silicates and oxides from microprobe analyses, using stoichiometric criteria. Mineralogical Magazine 51, 431–435.

Dubacq, B., Vidal, O., Andrade, V., 2010. Dehydration of dioctahedral aluminous phyllosilicates: thermodynamic modelling and implications for thermobarometric estimates. Contribution to Mineralogy and Petrology 159, 159–174.

Duretz, T., Agard, P., Yamato, P., Ducassou, C., Burov, E.B., Gerya, T.V., 2015. Thermo-mechanical modeling of the obduction process, based on the Oman ophiolite case. Gondwana Research (submitted for publication).

Ernst, W.G., McLaughlin, R.J., 2012. Mineral parageneses, regional architecture, and tectonic evolution of Franciscan metagraywackes, Cape Mendocino-Garberville-Covelo 30′ × 60′ quadrangles, northwest California. Tectonics 31. http://dx.doi.org/10.1029/2011TC002987.

Gessner, K., Collins, A.S., Ring, U., Güngör, T., 2004. Structural and thermal history of poly-orogenic basement: U–Pb geochronology of granitoid rocks in the southern Menderes Massif, Western Turkey. Journal of the Geological Society 161, 93–101.

Gnos, E., 1998. Peak Metamorphic Conditions of Garnet Amphibolites Beneath the Semail Ophiolite: Implications for an Inverted Pressure Gradient. International Geology Review 40, 281–304.

Goffé, B., Oberhänsli, R., 1992. Ferro- and magnesiocarpholite in the "Bündnerschiefer" of the eastern Central Alps (Grisons and Engadine window). European Journal of Mineralogy 2, 835–838.

Göncüoglu, M.C., Yalınız, M.K., Tekin, U.K., 2006. Geochemistry, tectono-magmatic discrimination and radiolarian ages of basic extrusives within the Izmir-Ankara suture belt (NW Turkey): time constraints for the Neotethyan evolution. Ofioliti 31, 25–38.

Green, E., Holland, T., Powell, R., 2007. An order-disorder model for omphacitic pyroxenes in the system jadeite-diopside-hedenbergite-acmite, with applications to eclogitic rocks. American Mineralogist 92, 1181–1189.

Gurnis, M., Hall, C., Lavier, L., 2004. Evolving force balance during incipient subduction. Geochemistry, Geophysics, Geosystems 5, Q07001.

Gutnic, M., Monod, O., Poisson, A., Dumont, J.-F., 1979. Géologie des Taurides occidentales (Turquie). Mémoires la Société géologique de France 137, 1–112.

Hacker, B.R., 1990. Simulation of the metamorphic and deformational history of the metamorphic sole of the Oman Ophiolite. Journal of Geophysical Research 95, 4895–4907.

Hacker, B.R., 1991. The role of deformation in the formation of metamorphic gradients: Ridge subduction beneath the Oman Ophiolite. Tectonics 10, 455–473.

Hacker, B.R., Peacock, S.M., Abers, G.A., Holloway, S.D., 2003. Subduction factory 2. Are intermediate-depth earthquakes in subducting slabs linked to metamorphic dehydration reactions? Journal of Geophysical Research 108, 2030.

Harris, N.B.W., Kelley, S., Okay, A.I., 1994. Post-collision magmatism and tectonics in northwest Anatolia. Contribution to Mineralogy and Petrology 117, 241–252.

Holland, T.J.B., Powell, R., 1998. An internally consistent thermodynamic data set for phases of petrological interest. Journal of Metamorphic Geology 16, 309–343.

Holland, T.J.B., Baker, J., Powell, R., 1998. Mixing properties and activity-composition relationships of chlorites in the system MgO-FeO-Al_2O_3-SiO_2-H_2O. European Journal of Mineralogy 10, 395–406.

Hyndman, R.D., Peacock, S.M., 2003. Serpentinization of the forearc mantle. Earth and Planetary Science Letters 212, 417–432.

Jolivet, L., Faccenna, C., Huet, B., Labrousse, L., Le Pourhiet, L., Lacombe, O., Lecomte, E., Burov, E., Denèle, Y., Brun, J.-P., Philippon, M., Paul, A., Salaün, G., Karabulut, H., Piromallo, C., Monié, P., Gueydan, F., Okay, A.I., Oberhänsli, R., Pourteau, A., Augier, R., Gadenne, L., Driussi, O., 2013. Aegean tectonics: Strain localisation, slab tearing and trench retreat. Tectonophysics 597–598, 1–33.

Kaya, O., 1972. Outlines of the ophiolite question in the Tavsanli region (in Turkish). Bulletin of the Geological Society of Turkey 15, 26–108.

Kaya, O., Kozur, H., Sadeddin, W., Helvaci, H., 2001. Late Norian age for a metacarbonate unit in NW Anatolia, Turkey. Geobios 34, 527–532.
Kirby, S., Engdahl, R.E., Denlinger, R., 1996. Intermediate-depth intraslab earthquakes and arc volcanism as physical expressions of crustal and uppermost mantle metamorphism in subducting slabs. Geophysical Monograph Series.American Geophysical Union, Washington, D. C.
Kretz, R., 1983. Symbols for rock-forming minerals. American Mineralogist 68, 277–279.
Leake, B.E., Woolley, A.R., Arps, C.E.S., Birch, W., Gilbert, C., Grice, J., Hawthorne, F.C., Kato, A., Kisch, H.J., Krivovichev, V.G., Linthout, K., Laird, J., Mandarino, J.A., Maresch, W.V., Nickel, E., Schumacher, J.C., Smith, D., Stephenson, N., Ungarette, L., Whittaker, E., Youzhi, G., 1997. Nomenclature of amphiboles: report of the subcommittee on amphiboles of the international mineralogical association, commission on new minerals and mineral names. European Journal of Mineralogy 9, 623–6514.
Lisenbee, A., 1972. Structural setting of the Orhaneli ultramafic massif near Bursa, Northwestern Turkey. (PhD thesis). Pennsylvania State University, USA.
Manav, H., Gültekin, A.H., Uz, B., 2004. Geochemical evidence for the tectonic setting of the Harmancik ophiolites, NW Turkey. Journal of Asian Earth Sciences 24, 1–9.
Marschall, H.R., Schumacher, J.C., 2012. Arc magmas sourced from mélange diapirs in subduction zones. Nature Geoscience 5, 862–867.
Moix, P., Beccaletto, L., Kozur, H.W., Hochard, C., Rosselet, F., Stampfli, G.M., 2008. A new classification of the Turkish terranes and sutures and its implication for the paleotectonic history of the region. Tectonophysics 451, 7–39.
Monié, P., Agard, P., 2009. Coeval blueschist exhumation along thousands of kilometers: Implications for subduction channel processes. Geochemistry, Geophysics, Geosystems 10, Q07002. http://dx.doi.org/10.1029/2009GC002428.
Monod, O., Andrieux, J., Gautier, Y., Kienast, J.R., 1991. Pontides-Taurides relationship in the region of Eskisehir (NW Turkey). Bulletin of the Technical University, Istanbul 44, 257–278.
MTA, 2002. Geological map of Turkey, scale 1:500,000, Izmir. Miner. Res. Explor. Inst. Turkey.
Myhill, R., 2011. Constraintes on the evolution of the Mesohellenic ophiolite from subophiolitic metamorphic rocks. Geological Society of America Special Papers 480, 75–94.
Nicolas, A., Le Pichon, X., 1980. Thrusting of young lithosphere in subduction zones with special reference to structures in ophiolitic peridotites. Earth and Planetary Science Letters 46, 397–406.
Nitsch, K.-H., 1972. Das P-T-XCO_2-Stabilitätsfeld von Lawsonit. Contribution to Mineralogy and Petrology 34, 116–134.
Okay, A.I., 1980a. Lawsonite zone Blueschists and a sodic amphibole producing reaction in the Tavşanlı Region, Northwest Turkey. Contribution to Mineralogy and Petrology 72, 243–255.
Okay, A.I., 1980b. Mineralogy, petrology and phase relations of Glaucophane-Lawsonite blueschists from the Tavşanlı region, northwest Turkey. Contribution to Mineralogy and Petrology 72, 243–255.
Okay, A.I., 1982. Incipient Blueschist metamorphism and metasomatism in the Tavşanlı Region, Northwest Turkey. Contribution to Mineralogy and Petrology 79, 361–367.
Okay, A.I., 1986. High-pressure/low-temperature rocks of Turkey. In: Evans, B.W., Brown, E.H. (Eds.), Blueschists and eclogites. Geological Society of America Memoir, pp. 333–347.
Okay, A.I., 2002. Jadeite – chloritoid – glaucophane – lawsonite blueschists in north-west Turkey: unusually high P/T ratios in continental crust. Journal of Metamorphic Geology 20, 757–768.
Okay, A.I., Kelley, S., 1994. Tectonic setting, petrology and geochronology of jadeite + glaucophane and chloritoid + glaucophane schsits from north-west Turkey. Journal of Metamorphic Geology 12, 455–466.
Okay, A.I., Tüysüz, O., 1999. Tethyan sutures of northern Turkey. Geological Society of London, Special Publication 156, 475–515.
Okay, A.I., Harris, N.B.W., Kelley, S., 1998. Exhumation of blueschists along a Tethyan suture in northwest Turkey. Tectonophysics 285, 275–299.
Okay, A.I., Satır, M., Shang, C.K., 2008. Ordovician metagranitoid from the Anatolide-Tauride Block, northwest Turkey: geodynamic implications. Terra Nova 20, 280–288.
Okay, A.I., İşintek, I., Altıner, D., Özkan-Altıner, S., Okay, N., 2012. An olistostrome–mélange belt formed along a suture: Bornova Flysch zone, western Turkey. Tectonophysics 568–569, 282–295.
Okay, A.I., Sunal, G., Sherlock, S., Altıner, D., Tüysüz, O., Kylander-Clark, A.R.C., Aygül, M., 2013. Early Cretaceous sedimentation and orogeny on the active margin of Eurasia: Southern Central Pontides, Turkey. Tectonics 32, 1247–1271.
Önen, P., 2003. Neotethyan ophiolitic rocks of the Anatolides of NW Turkey and comparison with Tauride ophiolites. Geological Society of London, Special Publication 160, 947–962.
Önen, A.P., Hall, R., 1993. Ophiolites and related metamorphic rocks from the Kutahya region, north-west Turkey. Geological Journal 28, 399–412.
Önen, P., Hall, R., 2000. Sub-ophiolite metamorphic rocks from NW Anatolia, Turkey. Journal of Metamorphic Geology 18, 483–495.
Önen, A.P., Hall, R., 2003. Neotethyan ophiolitic rocks of the Anatolides of NW Turkey and comparison with Tauride ophiolites, Geological Society, London. Special Publications 160, 947–962.
Page, F.Z., Armstrong, L.S., Essene, E.J., Mukasa, S.B., 2006. Prograde and retrograde history of the Junction School eclogite, California, and an evaluation of garnet–phengite–clinopyroxene thermobarometry. Contribution to Mineralogy and Petrology 153, 533–555.
Parrot, J.F., Whitechurch, H., 1978. Subduction antérieures au chariage nord-sud de la croute Téthysienne : Facteur de métamorphisme des séries sédimentaires et volcaniques liées aux assemblages ophiolitiques Syro-Turcs, en schistes verts et amphibolites. Revue de Géographie Physique et de Géologie Dynamique 20, 153–169.
Peacock, S.M., 1993. The importance of blueschist → eclogite dehydration reactions in subducting oceanic crust. Geological Society of America Bulletin 105, 684–694.
Peacock, S., 1996. Thermal and petrologic structure of subduction zones. In: Bebout, Gray E., Scholl, D.W., Kirby, S.H., Platt, J.P. (Eds.), Subduction: Top to bottom.
Peacock, S.M., Wang, K., 1999. Seismic consequences of warm versus cool subduction metamorphism: Examples from southwest and northeast Japan. Science 286 (80), 937–939.
Plunder, A., Agard, P., Dubacq, B., Chopin, C., Bellanger, M., 2012. How continuous and precise is the record of P-T paths? Insights from combined thermobarometry and thermodynamic modelling into subduction dynamics (Schistes Lustrés, W. Alps). Journal of Metamorphic Geology 30, 323–346.
Plunder, A., Agard, P., Chopin, C., Okay, A.I., 2013. Geodynamics of the Tavşanlı zone, western Turkey: Insights into subduction / obduction processes. Tectonophysics 608, 884–903.
Pourteau, A., Candan, O., Oberhänsli, R., 2010. High-pressure metasediments in central Turkey: Constraints on the Neotethyan closure history. Tectonics 29, TC5004.
Pourteau, A., Sudo, M., Candan, O., Lanari, P., Vidal, O., Oberhänsli, R., 2013. Neotethys closure history of Anatolia: insights from ^{40}Ar-^{39}Ar geochronology and P-T estimation in high-pressure metasedimentary rocks. Journal of Metamorphic Geology 31, 585–606.
Pourteau, A., Bousquet, R., Vidal, O., Plunder, A., Duesterhoeft, E., Candan, O., Oberhänsli, R., 2014. Multistage growth of Fe-Mg-carpholite and chloritoid, from field evidence to thermodynamic modeling. Contributions to Mineralogy and Petrology 168. http://dx.doi.org/10.1007/s00410-014-1090-7.
Rioux, M., Bowring, S., Kelemen, P., Gordon, S., Miller, R., Dudás, F., 2013. Tectonic development of the Samail ophiolite: High-precision U-Pb zircon geochronology and Sm-Nd isotopic constraints on crustal growth and emplacement. Journal Geophysical Research Solid Earth 118, 2085–2101.
Robertson, A.H.F., Dixon, J.E., Brown, S., Collins, A., Morris, A., Pickett, E., Sharp, I., Ustaomer, T., 1996. Alternative tectonic models for the Late Palaeozoic-Early Tertiary development of Tethys in the Eastern Mediterranean region. Geological Society of London, Special Publication 105, 239–263.
Rogers, G., Dragert, H., 2003. Episodic tremor and slip on the Cascadia subduction zone: the chatter of silent slip. Science 300, 1942–1943.
Sarıfakıoğlu, E., Özen, H., Winchester, J.A., 2009. Whole Rock and Mineral Chemistry of Ultramafic-mafic Cumulates from the Orhaneli (Bursa) Ophiolite, NW Anatolia. Turkish Journal of Earth Sciences 18, 55–83.
Schwartz, S., Guillot, S., Reynard, B., Lafay, R., Debret, B., Nicollet, C., Lanari, P., Auzende, A.L., 2013. Pressure–temperature estimates of the lizardite/antigorite transition in high pressure serpentinites. Lithos 178, 197–210.
Şengör, A.M.C., Yılmaz, Y., 1981. Tethyan evolution of Turkey: a plate tectonic approach. Tectonophysics 75, 181–241.
Servais, M., 1981. Données préliminaires sur la zone de suture médio-téthysienne dans la région d'Eskisehir (NW Anatolie). Comptes rendus l'Académie des Sciences 293, 83–86.
Sherlock, S., Kelley, S., 2002. Excess argon evolution in HP–LT rocks: a UVLAMP study of phengite and K-free minerals, NW Turkey. Chemical Geology 182, 619–636.
Sherlock, S., Kelley, S., Inger, S., Harris, N., Okay, A.I., 1999. Ar- 39 Ar and Rb-Sr geochronology of high-pressure metamorphism and exhumation history of the Tavsanli Zone, NW Turkey. Contribution to Mineralogy and Petrology 137, 46–58.
Singh, S.C., Carton, H., Tapponnier, P., Hananto, N.D., Chauhan, A.P.S., Hartoyo, D., Bayly, M., Moeljopranoto, S., Bunting, T., Christie, P., Lubis, H., Martin, J., 2008. Seismic evidence for broken oceanic crust in the 2004 Sumatra earthquake epicentral region. Nature Geoscience 1, 777–781.
Song, S.G., Zhang, L.F., Niu, Y., Wei, C.J., Liou, J.G., Shu, G.M., 2007. Eclogite and carpholite-bearing metasedimentary rocks in the North Qilian suture zone, NW China: implications for Early Palaeozoic cold oceanic subduction and water transport into mantle. Journal of Metamorphic Geology 25, 547–563.
Syracuse, E.M., van Keken, P.E., Abers, G.A., 2010. The global range of subduction zone thermal models. Physics of the Earth and Planetary Interiors 183, 73–90.
Tekin, U.K., Göncüoglu, M., 2009. Late Middle Jurassic (Late Bathonian-early Callovian) radiolarian cherts from the Neotethyan Bornova flysch zone, Spil Mountains, Western Turkey. Stratigraphy and Geological Correlation 17, 298–308.
Tekin, U.K., Göncüoglu, M., Turhan, N., 2002. First evidence of Late Carnian radiolarians from the Izmir–Ankara suture complex, central Sakarya, Turkey: implications for the opening age of the Izmir–Ankara branch of Neo-Tethys. Geobios 35, 127–135.
Topuz, G., Okay, A.I., Altherr, R., Meyer, H.-P., Nasdala, L., 2006. Partial high-pressure aragonitization of micritic limestones in an accretionary complex, Tavşanlı Zone, NW Turkey. Journal of Metamorphic Geology 24, 603–613.
Tsujimori, T., Matsumoto, K., Wakabayashi, J., Liou, J.G., 2006. Franciscan eclogite revisited: Reevaluation of the P–T evolution of tectonic blocks from Tiburon Peninsula, California, U.S.A. Mineralogy and Petrology 88, 243–267.
Ukar, E., Cloos, M., 2014. Low-temperature blueschist-facies mafic blocks in the Franciscan melange, San Simeon, California: Field relations, petrology, and counterclockwise P-T paths. Geological Society of America Bulletin 126, 831–856.
van der Kaaden, G., 1966. The significance and distribution of glaucophane rocks in Turkey. Bulletin Miner. Res. Explor. Inst. 67, 37–67.
van Hinsbergen, D.J.J., Kaymakci, N., Spakman, W., Torsvik, T.H., 2010. Reconciling the geological history of western Turkey with plate circuits and mantle tomography. Earth and Planetary Science Letters 297, 674–686.
van Keken, P.E., Hacker, B.R., Syracuse, E.M., Abers, G.A., 2011. Subduction factory: 4. Depth-dependent flux of H_2O from subducting slabs worldwide. Journal of Geophysical Research 116, B01401. http://dx.doi.org/10.1029/2010JB007922.
Vidal, O., Parra, T., 2000. Exhumation paths of high-pressure metapelites obtained from local equilibria for chlorite ± phengite assemblages. Geological Journal 161, 139–161.
Vidal, O., de Andrade, V., Lewin, E., Munoz, M., Parra, T., Pascarelli, S., 2006. P-T-deformation-Fe^{3+}/Fe^{2+} mapping at the thin section scale and comparison with XANES mapping: application to a garnet-bearing metapelite from the Sambagawa metamorphic belt (Japan). Journal of Metamorphic Geology 24, 669–683.

Wada, I., Wang, K., 2009. Common depth of slab-mantle decoupling: Reconciling diversity and uniformity of subduction zones. Geochemistry, Geophysics, Geosystems 10, Q10009.
Wakabayashi, J., 2013. Subduction initiation, subduction accretion, and nonaccretion, large-scale material movement, and localization of subduction megaslip recorded in Franciscan complex and related rocks, California. Geological Society of America Field Guide 32, 129–162.
Wakabayashi, J., Dilek, Y., 2003. What constitute 'emplacement' of an ophiolite?: Mechanisms and relationship to subduction initiation and formation of metamorphic soles. Geological Society of London, Special Publication 218, 427–447.
White, R.W., Powell, R., Holland, T.J.B., 2007. Progress relating to calculation of partial melting equilibria for metapelites. Journal of Metamorphic Geology 25, 511–527.
Woodcock, N.H., Robertson, A.H.F., 1977. Origins of some ophiolite-related metamorphic rocks of the "Tethyan" belt. Geology 5, 373–376.
Yoshioka, S., Mikumo, T., Kostoglodov, V., Larson, K.M., Lowry, A.R., Singh, S.K., 2004. Interplate coupling and a recent aseismic slow slip event in the Guerrero seismic gap of the Mexican subduction zone, as deduced from GPS data inversion using a Bayesian information criterion. Physics of the Earth and Planetary Interiors 146, 513–530.